1
Some Facets of Molecular Disorder in Crystalline and Amorphous Pharmaceuticals

Marc Descamps and Jean-François Willart

Most drugs, agrochemicals, and so on, are formulated in the solid state, which may be either crystalline or amorphous (i.e., glassy). It is well known that glassy compounds are very disordered solids. However, molecular crystals can also have varying degrees of disorder. Even perfect crystals are always disordered because of the thermal agitation of atoms and molecules. The intentional use of disordered solids and amorphous materials can be of great interest in pharmaceutical formulations because they may have favorable biopharmaceutical properties, for example, enhanced solubility and dissolution capabilities [1–3]. The drawback of this approach is that, often, the disordered solids can be metastable or unstable, physically or (and) chemically [4–6]. Glassy materials are in a nonequilibrium state and evolve upon aging. Formation of disordered solids may also be accidental, during the processing of crystalline materials. That can dramatically undermine the expected stability of the drug [7].

The differences in behavior between the different types of solids are fundamentally associated with the peculiarities of the molecular disorder. In the pharmaceutical literature related to amorphous solids, most interest has been focused on the molecular mobility and the way it may impact stability [8]. If mobility obviously plays an important role, many other aspects of the disorder also can determine the stability level of solids [9]. In this chapter we examine some of the facets of disorder that make it possible to differentiate between crystalline and amorphous states and also between various amorphous states of the same compound. That requires considering the structural, dynamic, thermodynamic, and even kinetic aspects of disorder.

Disordered Pharmaceutical Materials, First Edition. Edited by Marc Descamps.
© 2016 Wiley-VCH Verlag GmbH & Co. KGaA. Published 2016 by Wiley-VCH Verlag GmbH & Co. KGaA.

1.1
The Crystal/Amorph Alternative

1.1.1
Crystal/Amorph Alternative: Terminology and Solidity Concept

Condensed matter can normally come in two forms: liquid and solid. The distinction between liquid and solid states lies in how they respond to the application of a shear stress.

A liquid deforms continuously when it is subjected to a shear stress: it is a fluid form of condensed matter.

A solid, on the contrary, can support a shear stress without flowing. If the shear is not too strong, it will deform elastically. This means that when the external forces are removed, an elastically deformed solid returns to its initial state: it is a rigid form of matter.

Solids can be either crystalline or amorphous: they differ in their structure and in the way they are solid.

Perfect crystals are those in which a "motif" – formed by a limited number of atoms or group of atoms – is repeated periodically in a three-dimensional array (lattice). This is reflected in the specific external shape that the crystals can adopt. The equilibrium state of a material at low temperature is expected to be crystalline.

The amorphous state of a material does not possess the long-range translational order (periodicity) of a crystal. It has no specific external shape. A liquid is always amorphous, but amorphous materials can be either solid or liquid. Noncrystalline solids formed as the result of the deep undercooling of a liquid are conventionally called glasses.

Crystalline and amorphous solids are not solids in the same way:

- *Crystalline solids* are "real solids" in that the elastic reversibility does not depend on the length of time that the shear stress acts. The elastic behavior is characterized by the shear modulus G, which is the constant of proportionality between the strain and the applied stress.
- *Noncrystalline (amorphous) solidity* needs considering the viscoelastic property of a real liquid. Generally, a real liquid is capable of responding at first in an elastic way (instantaneous shear modulus G_∞). But, in the words of Maxwell [10], the elastic behavior is fugitive. After a given time τ ($\tau =$ relaxation time, which is a function of the temperature T), the behavior is that of a liquid. The behavior is then characterized by the viscosity $\eta(T)$. According to Maxwell's model [11], the value of τ is linked to that of η and G_∞ by

$$\tau = \eta / G_\infty \tag{1.1}$$

For liquid water at room temperature, $\tau \cong 10^{-3}$ Pa·s/10^9 Pa $= 10^{-12}$ s. This very low value of τ gives rise to a high effective fluidity. The designation of an amorphous compound as a liquid or solid depends on the value of τ relative to the

time of observation t_0. If $t_0 < \tau$, the material behaves as a solid. If τ becomes on the order of a few hours or days, a viscoelastic liquid can be considered operationally as a solid: it is a glass. G_∞ depends on the material and temperature, but its order of magnitude is always some gigapascals (GPa) or tens of GPa. When a liquid can be undercooled (i.e., cooled without crystallizing), the value of G_∞ is observed to vary with temperature. However, its temperature dependence is insignificant compared to the large temperature dependence of η. As a consequence, τ and η are roughly proportional. Values of $10^3 - 10^4$ s for τ correspond to viscosity values of about 10^{12} Pa·s ($\equiv 10^{13}$ poises). When the viscosity of an undercooled liquid – which fails to crystallize – reaches such values, we start observing a solid behavior. This marks the entry into the glassy domain. The glass transition temperature T_g has often been defined as that at which the viscosity of an undercooled liquid reaches a value of 10^{13} poise. We will later give another definition of T_g based on calorimetric observations.

1.1.2
Crystal/Amorph Alternative: Structural Order and Disorder

In this subsection we focus on the structural aspects of order and disorder. We are concerned about the relative positions and orientations of the molecules, ignoring the possible dynamic aspects of the disorder (molecular mobility). In a simple manner, an amorphous solid is sometimes defined as a "disordered solid"; however, crystals, even perfect, are always disordered at some level, and sometimes very disordered. On the other hand, the structure of many amorphous solids is, in fact, non-random at certain length scales. We will briefly discuss the various forms of disorders that will help us to specify the boundary between crystalline and amorphous disorders.

X-ray (and neutron) diffraction by a sample are probably the best techniques to provide direct information about the structural organization of condensed matter. The effects of the different types of disorders on X-ray diffractograms will be presented to help identifying them.

1.1.2.1 Perfect Crystals

A perfect crystal is the periodic repetition in three dimensions (in principle to an infinite extent) of unit cells containing an atomic or molecular motif composed of a few atoms only. The unit cell is built on three noncoplanar vectors $\mathbf{a}_1$, $\mathbf{a}_2$, and $\mathbf{a}_3$ (Figure 1.1). The structural situation at some point in space is exactly reproduced at every other point obtained by adding a lattice translation vector:

$$\mathbf{r}_m = m_1\mathbf{a_1} + m_2\mathbf{a_2} + m_3\mathbf{a_3}\cdot\ (m_1, m_2, m_3 \text{ are integers})$$

In brief, a crystal = a motif + a lattice.

The translational invariance defines the long-range order (LRO) of a crystalline state.

X-Ray diffraction by perfect crystals (for details, see [12–14])

The geometry of an X-ray diffraction experiment is shown in Figure 1.2.

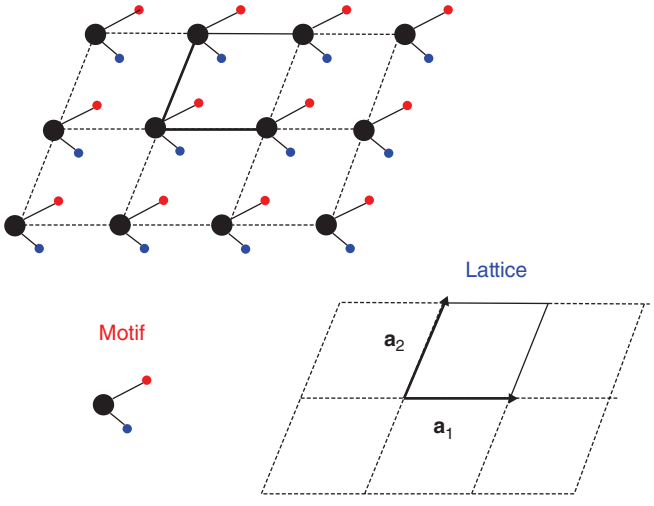

Figure 1.1 Two-dimensional representation of the periodic property of a molecular crystal.

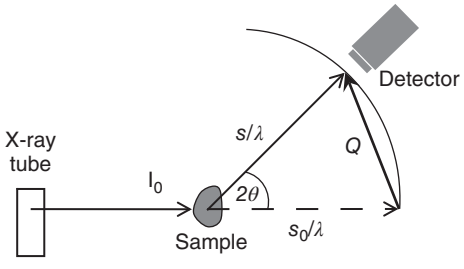

Figure 1.2 Usual setup for X-ray diffraction experiments. λ is the wavelength. **Q** is the scattering vector. $\mathbf{IQI} = |(\mathbf{s}-\mathbf{s}_0)/\lambda| = 2\sin(\theta)/\lambda$ $|\mathbf{s}|=|\mathbf{s}_0|=1$.

The general expression of the intensity diffracted by the atoms of a sample – whatever its structure, crystalline or not – is given by

$$I(\mathbf{Q}) = \Sigma_i \Sigma_j f_i f_j \exp[i\, 2\pi\, \mathbf{Q}\cdot (\mathbf{r}_i - \mathbf{r}_j)] \tag{1.2}$$

where **Q** is the scattering vector, which is a vector in the reciprocal space as defined in Figure 1.2. f_n is the atomic scattering factor of the nth atom of the sample situated at $\mathbf{r}_n$ from the origin. Summations are taken over the full sample. This expression simply shows that X-ray diffraction provides an image, in the reciprocal space, of the structure of the sample.

In the case of a perfect crystal, the translational repetition of the motif allows simplifying the expression of $\boldsymbol{I}(\mathbf{Q})$ in the form of a product:

$$I(\mathbf{Q}) = |F(\mathbf{Q})|^2 \cdot \mathfrak{I}(\mathbf{Q}) \tag{1.3}$$

$F(\mathbf{Q})$ is the *structure factor* of the unit cell. It reflects the distribution of positions of the molecules (the *motif*) within the unit cell relative to the lattice points.

$$F(\mathbf{Q}) = \Sigma_j f_j \exp[i2\pi\,\mathbf{Q}\cdot\mathbf{r}_j] \tag{1.4}$$

where the summation is taken on the atoms j of the unit cell only.

$\mathfrak{I}(\mathbf{Q})$ is called the *interference function.* It reflects the geometry of the *lattice.*

$$\mathfrak{I}(\mathbf{Q}) = \Sigma_m \Sigma_{m'} \exp[i\,2\pi\,\mathbf{Q}\cdot(\mathbf{r}_m - \mathbf{r}_{m'})] \tag{1.5}$$

where $\mathbf{r}_m$ is the vector specifying the origin of the mth unit cell. Summations are taken on the full sample.

- Because of the translational invariance, if the crystalline sample is very large, $\mathfrak{I}(\mathbf{Q})$ has nonzero values only for $\mathbf{Q}$ corresponding to nodes of the reciprocal lattice (RL) of the crystal [12–14]. This determines the positions of the Bragg peaks. If the size of the crystal is large enough (more than a few micrometers), the width of the $\mathfrak{I}(\mathbf{Q})$ function around each RL node is negligible.
- The intensity integrated over one diffraction line is proportional to the number of unit cells.
- The positions of the diffraction peaks are given in the θ scale by the Bragg law:

$$\sin(\theta) = n\lambda/2d_{hkl} \tag{1.6}$$

where n is an integer and d_{hkl} is the spacing of a given set of crystallographic planes. Equation 1.6 also shows that Bragg peaks are observed for $|\mathbf{Q}| = n/d_{hkl}$. The position of the Bragg peaks depends only on the parameters of the unit cell. The intensity of the diffraction measured at one Bragg peak depends on the spatial organization of the motif in the unit cell, via the value of the structure factor $F(\mathbf{Q})$.

1.1.2.2 **Crystal Size Effect**

No crystal is fully perfect because of its finite size. Very often, pharmaceuticals are formulated as powders. Processes used to obtain the powder (milling, drying, etc.) may either give rise to micro/nanocrystalline or amorphous grains with very important consequences on the stability and functionality of the final drug. It is thus important to have a method to identify the structural and microstructural nature of the grains. Reduction of size can also be the result of accumulation of dislocations, which subdivide the crystal into small crystalline domains that diffract independently. It must be, however, noted that crystallite size is most often not the same thing as the particle size. A particle can be composed of several small crystallites. Particle sizes are measured, for example, by light scattering rather than by X-ray scattering.

Crystal size reduction leads to a specific type of X-ray peak broadening. In practice, this broadening can be observed only for crystallite sizes lower than 0.1–1 µm. Such peak broadening is only linked to a broadening of $\mathfrak{I}(\mathbf{Q})$ around the RL node while $F(\mathbf{Q})$ is not modified. As a consequence, the integrated intensity is still proportional to the number of unit cells composing the nanocrystal.

The width of a diffracted line, in Q units, is inversely proportional to the number of unit cells (N) along that direction.

$$\delta Q \propto 1/L_{hkl} \quad \text{where} \quad L_{hkl} = Nd_{hkl} \tag{1.7}$$

The important point is that δQ does not change with the order of the line (i.e., with Q). If the line profiles are plotted on the 2θ scale, the equation relating the crystallite size L to the broadening $\delta(2\theta)$ of the line observed at Bragg angle θ_0 is given by the Scherrer equation

$$\delta(2\theta) \cong 0.9l\lambda/L \cos\ \theta_0 \tag{1.8}$$

For this type of plot, a specific cosine dependence of the width is observed. When the crystal sizes are very small, and the Bragg peaks very broad, a considerable overlapping of the peak wings can give rise to an apparent diffuse background, which should not be interpreted as such.

Figure 1.3 shows the diffractograms of the same crystalline compound for various crystal sizes. For the smallest size (~30 Å = 3 nm), the diffractogram can become very similar to that of the amorphous form. The interpretation in

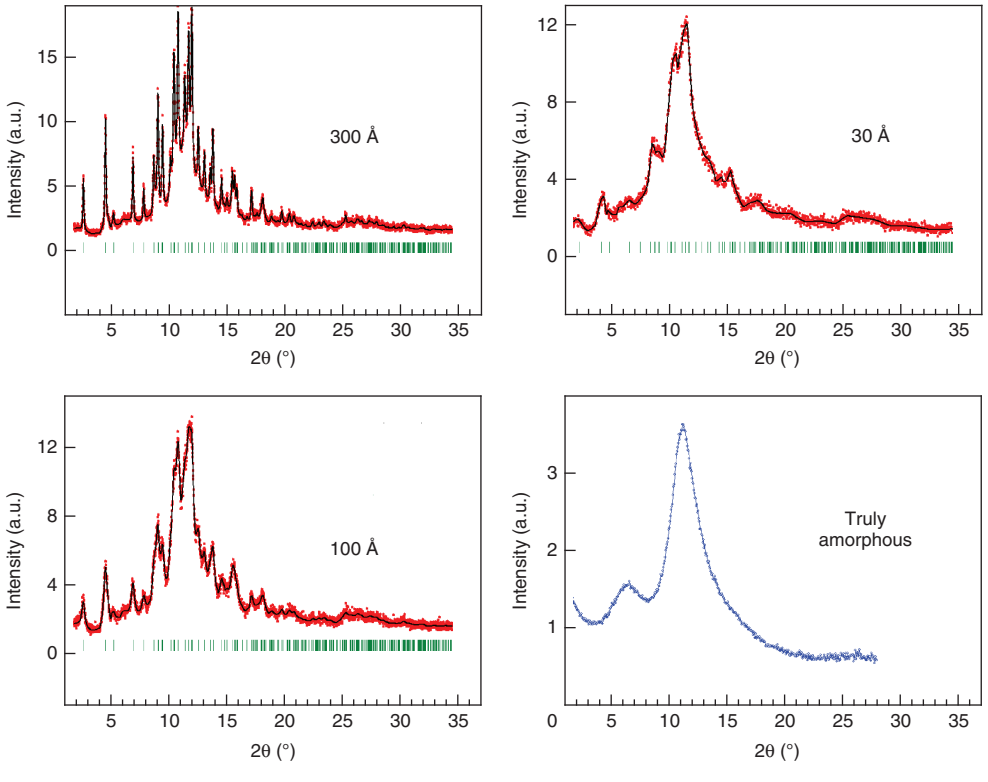

Figure 1.3 X-ray powder diagrams of the same molecular crystal for three different average sizes of the crystallites compared with the X-ray diagram of the fully amorphous form.

that case is challenging. Recent PDF (pair distribution function) analyses have made good progress in differentiating nanocrystalline and really amorphous compounds (for details see [15, 17] and the chapter by Bordet). When it is difficult to discriminate between an amorphous and a nanocrystalline situation, from the mere inspection of the X-ray diffraction pattern the presence or not of a calorimetric glass transition (existing only for the amorphous state) also helps in interpreting the structure.

1.1.2.3 Imperfect Crystals: How Disordered Can a Crystal Be?

The translational periodicity determines the LRO of crystals. However, some disorder or randomness is not necessarily incompatible with the crystalline nature. Such a disorder can arise from a local displacement of the structural elements (such as atoms, monomer units, motif) or a chemical substitution. A disorder induces fluctuations of the distance between homologous atoms. The characteristics of these fluctuations allow us to catalog crystalline imperfections and clarify the limit of crystallinity. In this respect, it is necessary to distinguish two kinds of crystalline imperfections [13, 14].

1) Imperfections of the first kind: They are such that the fluctuations of the interatomic (inter-motif) distances do not increase with the distance between motifs. Such imperfections preserve the long-range positional order of the lattice, on average. The motif that repeats translationally is an average one. This average is taken over either time or space.

$I(\mathbf{Q})$ can still be expressed in the form of the product shown in Eq. (1.3). The presence of $\mathfrak{I}(\mathbf{Q})$ still ensures the existence of Bragg peaks. Imperfections of the first kind do not induce broadening of the Bragg peaks. The structure factor is now an effective one: $<F(\mathbf{Q})>$.

It corresponds to the average motif, and takes into account all molecular positions inside the unit cell with an appropriate statistical weight. This type of disorder produces only a reduction in the intensity of the diffraction peaks at high Q values. The diffracted intensity removed from the Bragg peaks is spread throughout the reciprocal space in the form of a low-intensity, diffuse scattering.

Example 1.1. Thermal Agitation

The typical example of imperfection of the first kind is the thermal agitation of atoms and molecules that exist in every crystal. The regular positions of molecules in a crystal are only average positions around which they are continuously vibrating and librating. The centers of mass of the vibrating molecules are perfectly ordered because the vibrations of the different molecules are statistically similar. Figure 1.4 outlines a simplified example of a crystalline chain of atoms. It simply demonstrates how the fluctuations induced by vibrations are independent of the distance between the atoms. The amplitude of the fluctuation can be as large as 1/10 of the lattice parameter. It is highly temperature dependent. For X-ray diffraction, the atomic form factors have to be replaced by the temperature-dependent expression

$$f_j(T) = f_j \exp(-K\mathbf{Q}^2 \mathbf{u}_j^2) = f_j \exp(-M) \tag{1.9}$$

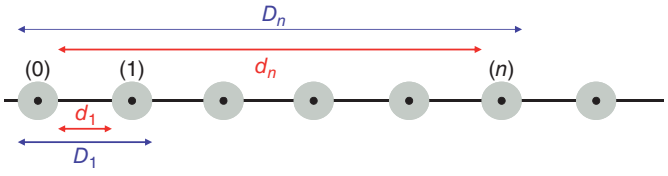

Figure 1.4 One-dimensional monoatomic model of imperfection of the first kind: thermal agitation. The gray zones show the spatial extension of atomic vibrations around the average position (black point). The fluctuation of the distances is independent of the interatomic distance: $D_1 - d_1 = D_n - d_n \; \forall \, n$.

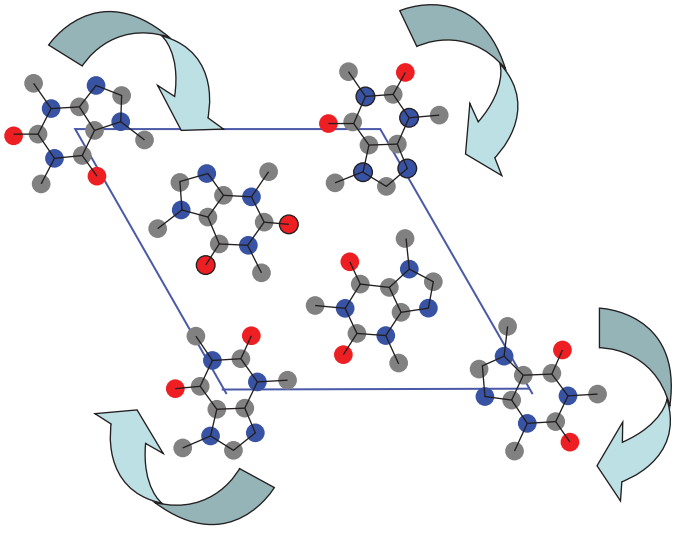

Figure 1.5 High-temperature hexagonal crystalline phase of caffeine. Molecules are rotating around the *C*-axis. The structure is perfectly crystalline but only on average.

where K is a constant and $\mathbf{u}_j$ is the average displacement of the atom.

M is usually called the Debye–Waller factor.

As a result of expression (1.9), $|F(\mathbf{Q})|^2$ and the Bragg scattering intensity are reduced. The reduction is more pronounced at high Q values (i.e., high Bragg angles) and for high temperatures where $\mathbf{u}_j^2$ is large.

Example 1.2. Rotationally Disordered Crystals ("plastic crystals") [18–20]

It is the case of the high-temperature crystalline phase of anhydrous caffeine [21]. Figure 1.5 shows the average hexagonal array of molecules. The high crystalline symmetry can be understood only if the caffeine molecules – which have a low symmetry – can rotate around their centers of mass. The dynamic aspect of this rotational disorder has been confirmed by dielectric relaxation experiments [21, 22]. Figure 1.6 shows the X-ray powder diffraction pattern of this phase [22]. It is characterized by very sharp peaks. The intensity of these peaks is, however,

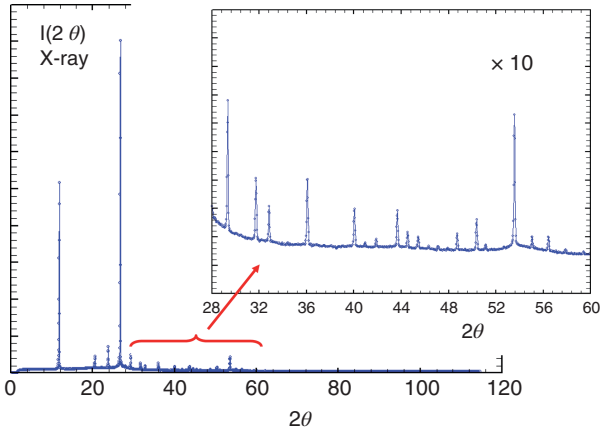

Figure 1.6 X-ray powder diagram of the high-temperature, hexagonal, disordered phase of caffeine. Notice the considerable decrease of peak intensities at high Bragg angle, which is due to the disorder. However, the Bragg peaks remains extremely sharp, which shows that the disorder is fully compatible with the existence of a perfect (average) crystalline periodicity.

decreasing fast with the Bragg angle. We can check that the width of the peaks does not increase with the diffraction angle. The situation is fully illustrative of the case of an imperfection of the first kind. The disorder is very important, but the crystal quality is very high.

We can notice the presence of a conspicuous diffuse scattering, which is spread in the angular range 10–30° (in 2θ). The diffuse scattering intensity corresponds to the intensity removed from the Bragg peaks due to the rotational disorder. This disordered crystalline phase is an example of mesophase. Other cases of mesophases are the liquid crystalline phases [23]. These latter types of mesophases are, however, no more crystalline. They are rather structured liquids (nematic, smectic, etc.).

Example 1.3. Ice Disorder

The crystalline polymorphism of ice is very complex, but the ordinary phase at atmospheric pressure (ice I_h) has a hexagonal structure, as shown in Figure 1.7a. The oxygen atoms form a regular hexagonal lattice, and each atom has four oxygen neighbors arranged tetrahedrally around it. One hydrogen atom resides along each bond connecting two neighboring oxygens. But each hydrogen lies close to one of the two oxygens and binds them. Each oxygen has two hydrogens close to it, which creates a local configuration similar to that of the H_2O molecule. However, the arrangement of hydrogens is not the same, but varies from one cell to another. The distribution of hydrogens is disordered: on each bond, the hydrogen atom can be closely bound to one or the other of the two oxygens. For the H_2O formula to be satisfied permanently, the jump of a hydrogen on one bond must entail a jump of another hydrogen on an adjacent bond. That is equivalent to saying that a water molecule can take six orientations around each oxygen site

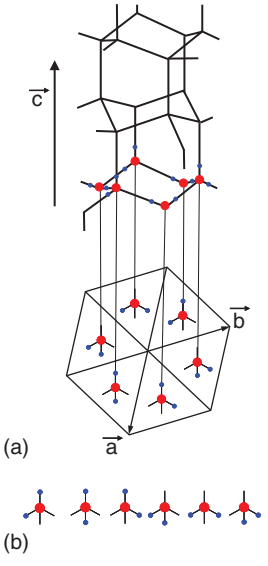

Figure 1.7 (a) Structure of hexagonal ice (I_h), showing the proton disorder. (b) The six possible configurations of a water molecule around each oxygen atom.

(Figure. 1.7b). That constitutes the Pauling "ice rules" [24, 25]. It is easy to imagine that the rotational motions of the water molecules are strongly coupled. The disorder of hydrogens and thus of water molecules is also manifested in the fact that the entropy of ice does not obey the third law of thermodynamics ($S(T = 0\,\mathrm{K}) \neq 0$: the well-known residual entropy of ice). As for other disordered crystals, the intensity of the diffraction peaks decreases at high Bragg angles. The neutron intensity away from the Bragg peaks is spread across the reciprocal space of the crystal in the form of a diffuse scattering. Because of the specificity of the ice disorder, as well as the strong intermolecular correlations resulting from the ice rules, the diffuse scattering takes the form of very specific patterns in the reciprocal space [25].

Example 1.4. Substitutional Disorder

The disorders outlined above are all related to shifts in atomic or molecular positions. There are also imperfections of the first kind, which result from chemical substitutions. These are molecular alloys in which two kinds of molecules can coexist in a same perfect average crystalline structure (Figure 1.8). The different molecular species that are present within the crystal, in a certain ratio, are mixed without any LRO. Note that the different molecular species can be the result of a conformational disorder of a given molecule (see chapters by Cesaro *et al.* and Coquerel *et al.*). Each unit cell can be described by an "average molecule." The atomic positions are determined, but the description of the unit cell – of the motif – needs introducing a statistical weight corresponding to the molecular ratio. Such a system is a crystalline solid solution. An important example is the chiral compounds that exhibit a so-called pseudo-racemic crystalline phase (sometimes called pseudo-racemate or racemic solid solution). Contrary to the racemic compounds or the conglomerates, the two enantiomers coexist in the crystal lattice but not in an ordered manner [26].

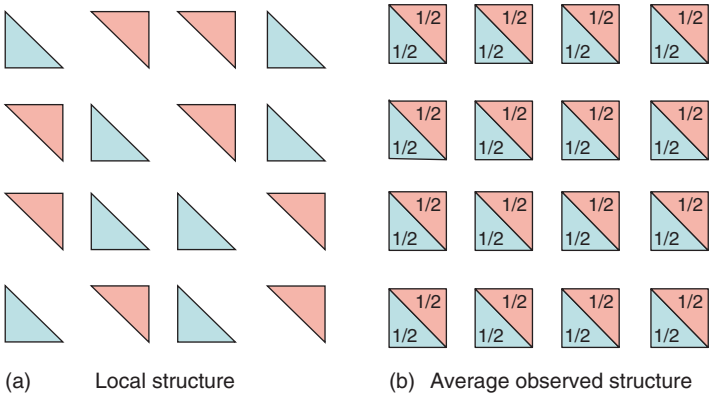

Figure 1.8 Two-dimensional illustration of a crystalline solution. Real local structure (a) and average structure (b) as determined by X-ray diffraction analysis.

2) Imperfections of the second kind: They are such that the fluctuations of the inter-motif distances increase with the distance between motifs. In that case, there is no more strict long-range crystalline periodicity or average motif.

When the fluctuations increase only very slightly, the molecular positioning is still rather well defined, though not perfect. The solid is then often designated as "badly crystallized". Sometimes, a "paracrystalline" description [16] can be adopted.

The X-ray diffraction of such a disordered system still shows a sort of diffraction peaks, which are however broadened. Unlike size broadening, the peak width δQ *increases with the order of the line* (i.e., with Q). The peak intensity also decreases rather fast as $|Q|$ increases.

Figure 1.9a gives a one-dimensional illustration of an imperfection of the second kind [13, 14]. Two kinds of atoms, with slightly different diameters, are stacked randomly. It is clear that in this case the fluctuation of the interatomic distance increases with the distance: $D_n - d_n > D_1 - d_1 (n > 1)$.

Figure 1.9b shows the X-ray picture corresponding to this system (in Q units). Pseudo-diffraction peaks are clearly visible. However, their width increases very rapidly with the order of the peak (as the square of the scattering vector $\mathbf{Q}^2$). At the same time, the maximum intensity decreases as $1/\mathbf{Q}^2$, so that only the first orders are observable. If the atomic scattering factors of the two types of atoms are different, the peaks are dissymmetric and their maxima are displaced from ideal reciprocal lattice nodes. By comparison, the peak width due to crystal size is independent of the peak index.

Another interesting situation corresponds to that of a collection of crystals with parameters that fluctuate around an average value. In that case, the peak broadening is proportional to $|\mathbf{Q}|$.

For solids of that type, which are often designated as "defective" crystals, line broadening analysis allows characterizing the microstructure and the type of

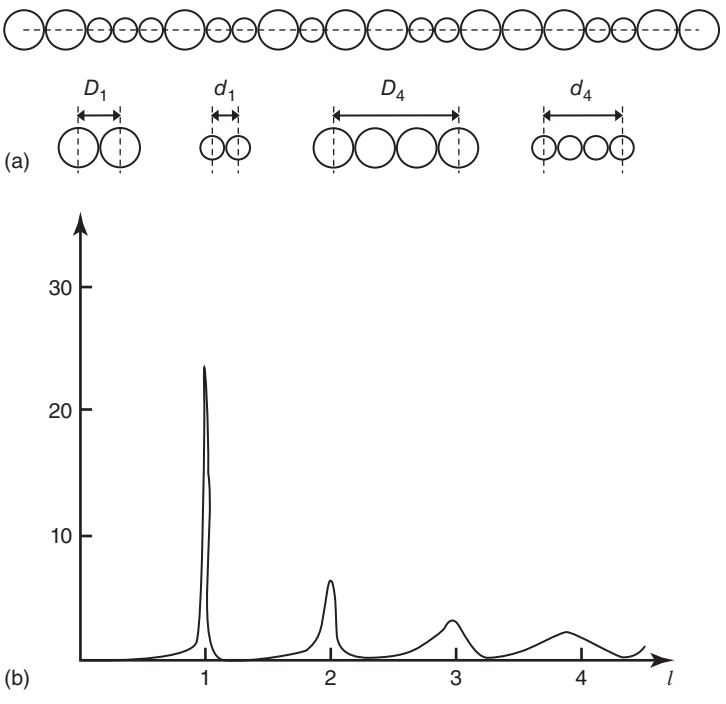

Figure 1.9 (a) One-dimensional illustration of an imperfection of the second kind [16]. Two types of atoms, with slightly different diameters, are stacked randomly. The fluctuation of the interatomic distance increases with the atomic separation [13]. (b) Corresponding calculated X-ray diagram [13, 14, 27].

disorder and identifying possible crystal size reductions. Many sophisticated software are available for this purpose (see the chapter by Bordet).

1.1.2.4 **Structure of Amorphous – Liquid or Glassy – Materials**

In these materials, the fluctuations increase so fast that any reference to a crystalline organization is difficult to make. It is the extreme form of imperfections of the second kind. The diffractograms have smooth variations because of a lack of strong interference effect. Figure 1.10 (bottom) shows the neutron diffraction pattern of amorphous ice. The profile has the particulars of what has been just described, but driven to the extreme: (i) considerable line broadening and (ii) fast increase in broadening with the order of the line. If an attempt is made to interpret the neutron diffractogram in terms of a nanocrystalline picture, the Bragg law (1.6) and Scherrer equation (1.8), respectively, give a repeat distance ($d \sim$ inverse of the first peak position) and a correlation length ($D \sim$ inverse of the peak width). This kind of brief analysis would predict a ratio $D/d \leq 3$. This value is much smaller than expected to consider the notion itself of crystallite being applicable. A statistical description of the structure is, therefore, preferred. In this frame, the structure is specified by the space variation of the radial pair distribution function (PDF) $g(r)$,

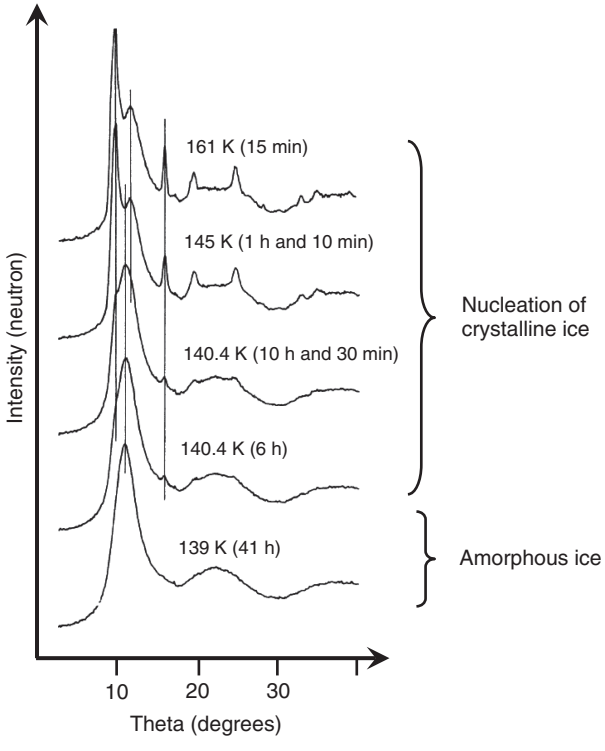

Figure 1.10 (Bottom) Neutron intensity measurement for low-temperature amorphous ice. The top diagrams, obtained upon heating, show the appearance of Bragg peaks corresponding to the progressive nucleation of crystalline ice (From Elarby *et al*. [28], Figure 1.10. Reproduced with permission).

which gives the probability of finding an atom at the distance r from another one. Experimental determination of $g(r)$ allows describing the short-range order (SRO) that possibly develops between the molecules.

Figure 1.11 illustrates the meaning of $g(r)$ in the case of a very simple monoatomic amorphous system.

The formalism to calculate the diffracted intensity $I(\mathbf{Q})$ is similar to that previously given (Eq. (1.2)). The difference is that the decomposition into the unit cell and lattice no longer makes sense, nor is the expression of $I(\mathbf{Q})$ in the form of a product. The average intensity $I(Q)$ can be expressed by introducing the average PDF $g(r)$. If we assume that all atoms in the sample are similar,

$$< I(Q) > \propto 1 + \rho_0 \int (g(r) - 1) 4\pi r^2 [\sin(2\pi Qr)/2\pi Qr]\, dr \tag{1.10}$$

where ρ_0 is the average value of density (for details see [14, 15] and the chapter by Bordet).

The formalism can be extended to polyatomic and molecular amorphous compounds in a rather straightforward way. The notation is, however, heavier. The

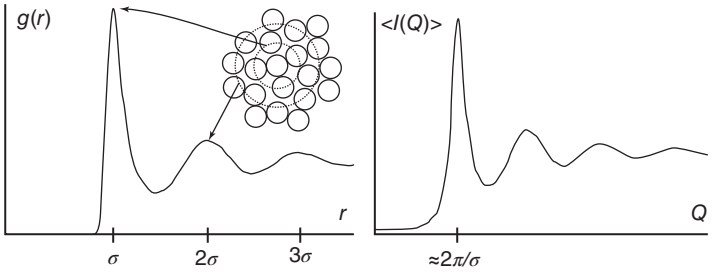

Figure 1.11 (a) Radial pair distribution function (PDF) $g(r)$ for a simple atomic liquid (atomic diameter σ). (b) The corresponding diffracted intensity $<I(Q)>$. A sample structure is also depicted where the solvation shells are indicated by the dotted lines. The exclusion radius can be seen in the absence of amplitude of $g(r)$ for $\sigma < r < 2\sigma$.

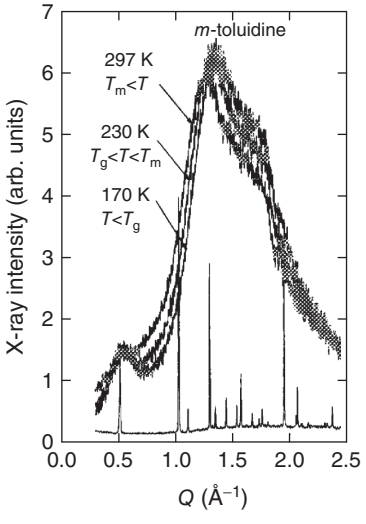

Figure 1.12 X-ray diffraction patterns of *meta*-toluidine. Liquid state: 297 K, undercooled liquid 230 K, glassy state 170 K. Crystalline phase: 230 K. (From Descamps *et al.* [32], Figure 1.12. Reproduced with permission of Progress of Theoretical Physics.)

PDF analysis is based on this formalism. It is widely used for amorphous compounds. It can also be used to investigate nanocrystalline materials. It is the case when the crystallite size becomes so small that distinction with a real amorphous state becomes dubious (cf. Figure 1.3). For details, see [28–31] and the chapter by Bordet. There are some cases where the simple observation of the diagram can give useful information. It is the case, for example, when a "pre-peak" is observed at a Bragg angle smaller than that of the main halo. In the real space, it is an indication of the formation of an intermediate range order that develops in the amorphous system. Such pre-peaks have been observed for several amorphous molecular compounds such as *meta*-toluidine and *meta*-cresol (Figure 1.12) [32]. Their presence suggests the formation of small clusters of chemically associated molecules [32, 33].

1.1.3 Crystal/Amorph Alternative: Metastability and Interconversion

1.1.3.1 Thermodynamic Measure of Physical Stability, Driving Force, Disorder

At given pressure, a crystal melts at temperature T_m. The melted compound – which is amorphous – can be undercooled below T_m with more or less ease. The possible existence below T_m of two states, namely crystalline or amorphous, poses the question of the relative stability of these states and of the rates at which the conversion between the two can occur. For transformations that occur at a given T and P, the stability of a state is measured by the Gibbs free energy (G), also named free enthalpy. G is defined by

$$G = H - TS \tag{1.11}$$

The differential form of $G(T,P)$ when T and P vary is given by

$$dG = -SdT + VdP \tag{1.12}$$

Here, H is the enthalpy, which measures the heat content of the system, and is reflective of its mechanical energy. T is the absolute temperature. S is the entropy of the system, which measures the level of molecular disorder. The value of G can be calculated using the measured values of the specific heat $C_p(T)$. The most stable state is that for which the Gibbs function is the lowest. The equilibrium value of G is a compromise between a low mechanical energy and a high disorder. Figure 1.13 shows a schematic variation of G with the molecular configurations at a given temperature T. Stable states correspond to minima. The lowest minimum corresponds to a stable configuration, and the highest to a metastable one.

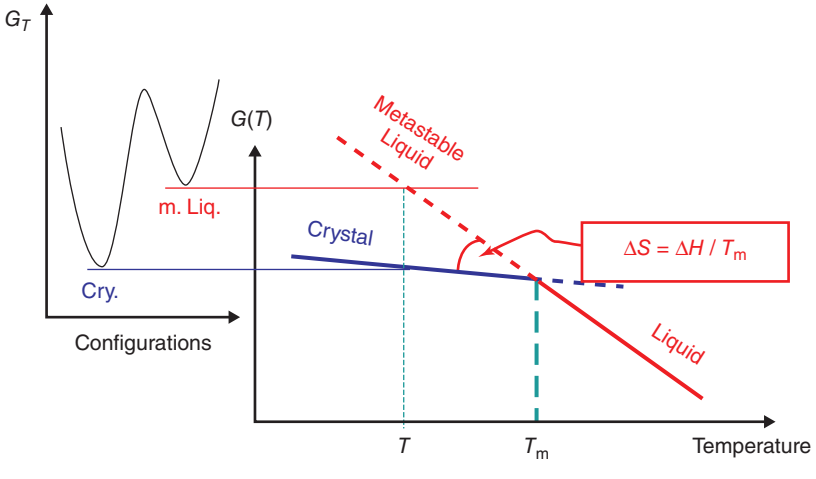

Figure 1.13 Schematic variations of the isothermal Gibbs curve as a function of molecular configurations for $T < T_m$. Stable states correspond to the minima. The figure also shows the evolution with temperature, in isobaric condition, of the free enthalpy curves of crystal and liquid phases.

Figure 1.13 also shows the evolution with temperature, under isobaric condition, of the free enthalpy curves of crystal and liquid phases. At the "equilibrium" melting temperature T_m, the values of G of the two phases are equal. The derivatives of $G(T)$ (which is $-S$) has a step change due to the increase in entropy (i.e., in disorder) ΔS_m when passing from the low-temperature crystal phase to the high-temperature liquid phase. Equality of the values of G for the two phases also means the existence of a latent heat ($\Delta H_m = T_m \cdot \Delta S_m$) for the transformation. Below T_m, the liquid state, which has a higher value, is metastable with respect to the crystal. In dealing with crystallization, we are concerned with the difference in G values between the two phases. Crystallization will be accompanied by a decrease in free enthalpy ΔG ($J\,mol^{-1}$). This ΔG decrease is the driving force for crystallization. At T_m, $\Delta G_m = 0$. Consequently crystallization cannot occur exactly at T_m. ΔG increases with the undercooling ($\Delta T = T_m - T$). A nonzero value of ΔG and, consequently, a minimum degree of undercooling ($\Delta T = T_m - T$) are necessary for a crystallization from the melt to occur. For small undercooling, and ignoring the difference in the specific heats of the liquid and crystal, a useful approximate expression of ΔG can be obtained:

$$\Delta G(T) \cong \Delta S_m \cdot \Delta T \cong \Delta H_m \, \Delta T / \, T_m \tag{1.13}$$

An exact expression should take into account the difference in heat capacity of the liquid and crystal, which is nonzero and especially large for the molecular compounds with which we are concerned. This difference is of the order of the magnitude of the heat capacity jump observed at the glass transition temperature, as will be shown later.

If a thermodynamic driving force is a prerequisite for a crystallization to occur, it is not its value alone that determines the occurrence and rate of the transformation itself. Several other factors play significant roles. In what follows, we discuss the interplay between the three main factors that determine the kinetics of recrystallization of an undercooled liquid and therefore determine the lifetime of metastability. In addition to the crystallization thermodynamic driving force, these factors are the liquid molecular mobility and the similarity in structure between the liquid and crystal (in particular near the interface).

1.1.3.2 Stability of the Amorphous State, Kinetics of Crystallization

The physical stability of the amorphous state is governed by the crystallization [34]. Crystallization occurs in the domain of metastability of the undercooled liquid ($T < T_m$). An amorphous, undercooled compound can be maintained in a metastable state for a length of time that depends strongly on the temperature. An understanding of the lifetime of metastability requires the investigation of the kinetics of recrystallization at each temperature. The progress of an isothermal crystallization as a function of time and temperature can be conveniently represented by the TTT (time, temperature, transformation rate) diagram, as shown in Figure 1.14 for the specific example of L-arabitol [35]. Specific isothermal experiments, which are sensitive to crystallization (DSC (differential scanning calorimetry), X-ray, dielectric measurement, etc.), allow us to plot such curves. A TTT

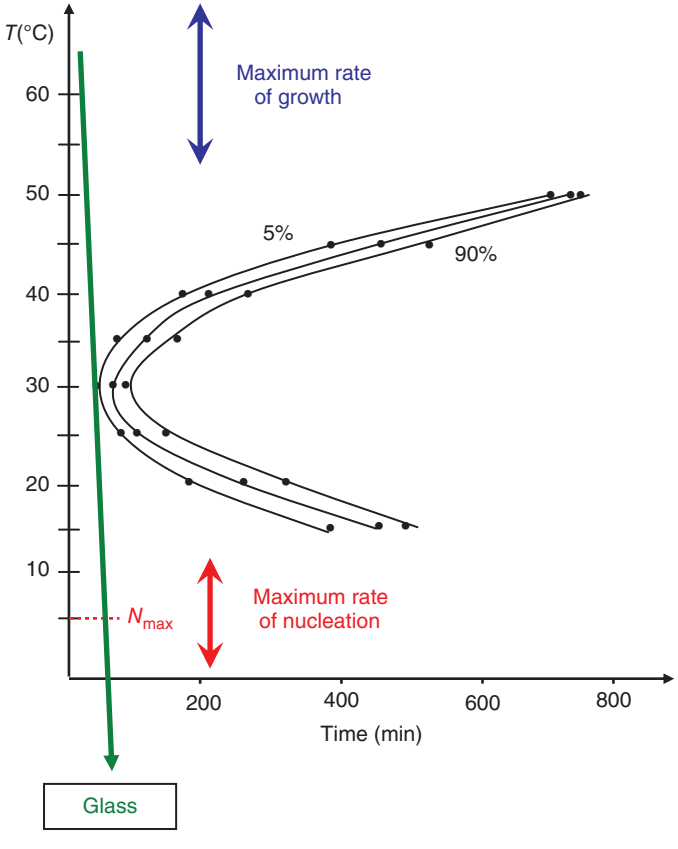

Figure 1.14 TTT (time, temperature, transformation rate) diagram for the specific example of L-arabitol. Also shown are the zones of maximum rate of nucleation (*N*) and growth (*V*). (From Descamps and Dudognon [35], Figure 1.14. Reproduced with permission of Wiley.)

diagram usually shows a nose-shaped feature of most rapid crystallization at some temperature. The overall behavior can be explained by the fact that the crystallization rate decreases when approaching the equilibrium melting temperature T_m because the thermodynamic driving force also decreases. At temperatures lower than that of the nose, the crystallization time increases as the molecular mobility decreases when approaching T_g. Going into detail, this description is too simplistic. Crystallization does not operate by a progressive homogeneous ordering process involving the entire sample at the same time. Crystallization of an undercooled amorphous melt results from the complex interplay between nucleation and growth processes. Nucleation is the process by which crystalline clusters having a minimum critical size appear randomly, with a given rate N (with dimension $t^{-1}L^{-3}$ in the usual 3D space), within the amorphous matrix. Once formed, the crystalline grains grow with a domain wall velocity V (with dimension $t^{-1}L$).

The combination of these two processes appears, for example, in the expression of the simplest JMAK (Johnson – Mehl – Avrami – Kolmogorov) model for the isothermal time (t) evolution of the fraction of crystallized material, $X(t)$ [36]:

For homogeneous nucleation and isotropic 3D growth

$$X(t) = 1 - \exp -[K(t/t_0)^4] \quad K = 4\pi/3 \tag{1.14}$$

This is a universal sigmoïdal function of the timescale

$$t_0 = (NV^3)^{-1/4} \tag{1.15}$$

where 4 ($=d+1$ where d is the dimensionality of the space in which the nucleation and growth transformation is proceeding) is the Avrami exponent. The temperature variation of t_0, which determines the shape of the TTT curve (Figure 1.14), depends on the rates of the nucleation and growth processes that have their proper temperature variations. Both have a maximum at some degree of undercooling. However, the two maxima do not occur at the same temperature, as shown in Figure 1.14. The maximum of $N(T)$ usually occurs slightly above T_g [37, 38], whereas the maximum of $V(T)$ occurs at a higher temperature often not far below T_m [39]. The width of the temperature gap between the nucleation and growth zones is important in determining whether a compound is a good glass former or not. It is also a determining factor in the physical stability of the amorphous compound.

Figure 1.15 shows the DSC curves recorded upon reheating an L-arabitol sample previously undercooled to temperatures $T_a < (T_m \cong 100\,^\circ\mathrm{C})$ ranging from -83 to $82\,^\circ\mathrm{C}$. No calorimetric events can be observed on the DSC heating curves for samples annealed at $T_a > 35\,^\circ\mathrm{C}$. The absence of any crystallization exotherm or melting endotherm shows that no crystallization process occurred during the cooling/heating cycle. Similarly, for $T_a < -10\,^\circ\mathrm{C}$, crystallization exotherms are not detectable. On these curves, we can see the localization of the glass transition temperature at $T_g \approx -12\,^\circ\mathrm{C}$. These results show that the sample was totally amorphized during cooling. On the contrary, for annealing temperatures T_a ranging between -5 and $30\,^\circ\mathrm{C}$, pronounced crystallization exotherms, followed by melting endotherms, are observed. The exotherms have their maxima located not far below the melting point, in the range $60-95\,^\circ\mathrm{C}$, that is, at temperatures clearly separated from the annealing T_a domain. The interpretation of these results is that the exotherms correspond to the growth of crystals nucleated at a significantly lower temperature. Figures 1.14 and 1.15, respectively, show the estimated localization of the maxima of $N(T)$ (N_{max}) and $V(T)$ (V_{max}) and their positions with respect to the nose of the TTT curve. That underlines the relative influence of the factors that contribute to the recrystallization.

Both $N(T)$ and $V(T)$ have a maximum, which results from the antagonistic effects of

1) The thermodynamic driving force, which increases when the degree of undercooling increases;
2) The molecular mobility, which decreases when the temperature decreases.

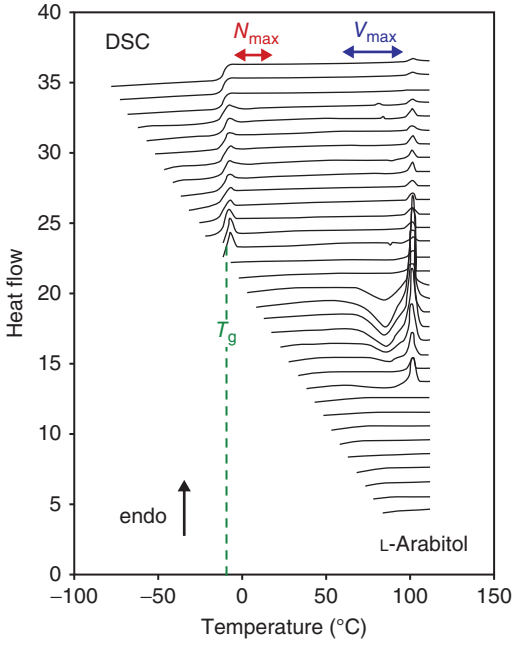

Figure 1.15 (L-Arabitol) DSC curves recorded upon heating (heating rate of 2 K min^{-1}) for samples undercooled at temperatures T_a ranging from −83 to 82 °C and annealed for 60 min at this temperature. (From Descamps and Dudognon [35], Figure 1.15. Reproduced with permission of Wiley.)

The latter prevails at low temperatures and becomes the limiting factor which permits to avoid the crystallization when quenching a liquid rapidly enough. The correlation between the decrease of $N(T)$ and $V(T)$ and the decrease of molecular mobility at low temperature has been shown in [35, 37] for indomethacin. The temperature positions of N_{max} and V_{max}, however, differ, mainly because of the effect of the surface tension γ between the crystallite starting to form and the amorphous metastable matrix. This is reflected in the expressions of $N(T)$ and $V(T)$ resulting from conventional theories [36, 40–44]:

- The classical "capillary" nucleation theory for $N(T)$ can be written in the form

$$N(T) = f_0(T) \exp(-g^*_{3-d}/RT) \tag{1.16}$$

The mobility term f_0 is an "attempt frequency" for the addition of molecules from the metastable melt to the stable crystal across the interface. The thermodynamic effect is expressed in the exponential factor. $g^*_{3-d} = 16\pi\gamma^3/3\Delta G^2$ is the nucleation barrier. This expression results from the competition between an unfavorable, positive interfacial free enthalpy (γ) and the negative bulk driving force (ΔG).

- The semiphenomenological expression of Turnbull [45] for $V(T)$ can be written in the form

$$V(T) \propto V_0(T) \cdot \Omega \cdot [1 - \exp(-\Delta G/RT)] \tag{1.17}$$

The mobility term $V_0(T)$ plays a role similar to that of f_0. The term inside the brackets expresses the influence of the thermodynamic driving force ΔG on the net flux from the amorphous matrix to crystal. Ω is a function of ΔG and depends on the specific mechanism of growth. γ has a strong impact on $N(T)$ via $g^*{}_{3-d}$ but has no (or limited for lateral growth) explicit influence on $V(T)$. The temperature separation of the preferential areas of nucleation and growth is mainly influenced by the value of the interfacial free enthalpy (γ). A high value of γ contributes to an increase in the distance between the two maxima N_{max} and V_{max} [35]. Because of this distance, and since N and V combine to give the characteristic time of the global kinetics t_0, the temperature variation of the latter is often connected to more than one cause. At low temperature, the decrease of molecular mobility has certainly a dramatic influence. However, due to the separation of $N(T)$ from $V(T)$, the effect of mobility on t_0 will result of a combination of factors, which have different temperature evolutions.

1.1.3.3 The Interfacial Free Enthalpy γ: Structure Dependence and Disorder Effect

It is useful to briefly address the molecular origin of the surface tension γ in order to better identify what can make a compound a good glass former. The value of γ is strongly influenced by the difference in the degree of order (disorder) between the amorphous mother phase and the crystallites, especially in the interfacial region. The surface tension γ is a free enthalpy (Gibbs free energy), and as such has an energetic and entropic contribution. Turnbull [45], Spaepen [46], and Oxtoby [47] pointed out that molecules of the liquid have to increase their ordering near the crystal boundary in order to optimize fitting with the translational order of the crystal and eventually allow an ordered embryo to grow. The entropy loss corresponding to this interfacial ordering is mainly the origin of the crystal/melt interfacial free enthalpy. Spaepen justified the fact (at least for atomic compounds) that entropy rises more slowly than enthalpy when going from a crystal to the bulk liquid. That is taken into account in the negentropic model [46, 48] of the interface. It provides an interesting guide to understanding the important and potential role of the relative disorder in the crystal embryo and relative order in the surrounding liquid.

Figure 1.16 summarizes schematically the situation. It shows the evolution of molecular ordering in the liquid at the interface and of the corresponding physical quantities, namely the enthalpy H and entropy S. At T_m, for example, there is a balance between enthalpic and entropic effects such as $\Delta H_m = T_m \Delta S_m$. At the interface, the balance is no longer satisfied, which gives rise to the excess free enthalpy γ. The maximum value of γ is obviously $\Delta H_m = T_m \Delta S_m$(bulk). At the interface, the molecular organization locally decreases the configurational entropy jump, which becomes ΔS(interface) $< \Delta S$(bulk).

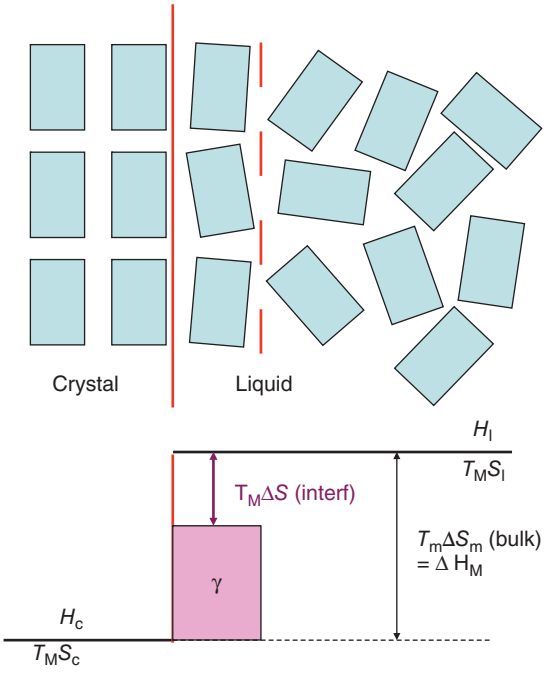

Figure 1.16 Schematic representation of the crystal/liquid interface showing short-range molecular ordering. The corresponding evolution of entropy that illustrates the negentropic approach of Spaepen (see Ref. [46, 48]).

The difference in free enthalpy (per molecule at the interface) between the liquid, which develops an interface, and that of the reference bulk is: T_m $[\Delta S(\text{bulk}) - \Delta S(\text{interface})]$.

Spaepen [46, 48] proposed the following formal expression for γ:

$$\gamma \propto \alpha T \Delta S_m \quad \text{with} \quad \alpha = [\Delta S(\text{bulk}) - \Delta S(\text{interface})]/\Delta S_m (< 1) \tag{1.18}$$

The above considerations allow us to understand some of the main factors that make a compound easy to undercool, or not, from the liquid state.

If the melting entropy is low, the maximum value of the crystal/melt surface tension will also be low, and the undercooling ability will be often very poor. This is the case for crystals that are very disordered, such as plastic crystals [18–20]. It is also the case recently found for the high-temperature phase of caffeine [21, 22, 49], and the reason why metastable polymorphic varieties (in a monotropic situation), which have lower melting enthalpies than the stable phase and thus higher crystalline entropies, are often the first to nucleate. The first crystalline phase to appear is not that of highest thermodynamic driving force but that of highest entropy. It is a way to justify the observations made by Oswald, as set out in his "rule of stage" [50, 51].

Poor undercooling ability is also found in the case of molecular liquids that are locally organized in a way mimicking crystalline order. In this case, much further

molecular organization is not needed at the interface. That leads to a low value of α. Turnbull and Spaepen used this argument to explain the small undercooling ability of *n*-alkane liquids [45]: The occurrence of linear configurations in the melt minimizes the entropy loss when adjusting to the crystal plane.

On the contrary, in the case of racemic compounds for example, the melt is a muti-component mixture of the *R* and *S* species. The entropy of melting is thus rather high. The ordered racemic compound is very difficult to nucleate from the melt, because a specific molecular organization is to be built at the interface that is costly in entropy. The first crystalline phase to appear is often a disordered solid solution of the *R* and *S* species. That seems to be the case recently found for racemic ibuprofen [35, 52, 53].

1.1.3.4 **Concluding Remarks**

Several factors may influence the recrystallization from the melt and thus play a role in the stability of the amorphous systems. These factors often compete in a delicate way. These are as follows:

- The thermodynamics that drives the process.
- The molecular mobility that facilitates (or not) the transformation.
- The interface energy that modulates the splitting of nucleation and growth processes. The interface energy is basically related to the structural similarity between bulk liquid, crystal, and the interface region between the two.
- The heterogeneities and cracks that may amplify considerably the rate of transformation. The role of these heterogeneities results from modifications of interface energy [36] and surface mobility [54, 55].

It should always be borne in mind that these different factors play a role when trying to interpret or to predict the stability behaviors of amorphous compounds.

Molecular compounds may exhibit a rich crystalline polymorphism with different structures and levels of disorder. The structural similarity with the liquid and the condition of recrystallization are modified accordingly. That plays a significant role in the phase selection.

1.1.4
Crystal/Amorph Alternative in the Context of Solubility

The low bioavailability of the active pharmaceutical ingredient (API), which is due to its poor solubility in water, is a major issue in pharmaceutical science. The use of the amorphous rather than crystalline form of API is considered one of the best formulation strategies to enhance the oral bioavailability. The principal reason that has long been recognized is that the amorphous state offers a way to extraordinarily increase the apparent aqueous solubility of poorly soluble pharmaceuticals [1, 5, 56–58]. Amorphous solid dispersion technologies have been emerging in the past years [59] in order to overcome the intrinsic instability of the amorphous state, both in the dosage form and during supersaturation in the intestinal environment. More recently, it has been shown that the use of the amorphous forms,

which allow increasing the apparent solubility without the addition of a solubilizer (co-solvents, surfactants, cyclodextrines, etc.), can concomitantly increase the drug flux through the intestinal membrane and thus provide higher overall absorption [60–63]. This could have a significant impact on oral drug delivery of lipophilic compounds.

In this subsection, we identify the reasons for the higher apparent solubility of the amorphous solid form of a pharmaceutical compound compared with that of a stable crystal form. Traditionally, the term "solubility" refers to the equilibrium limit of solubility of the stable crystalline form in a solvent (in practice, water for pharmaceutical applications). It is the maximum concentration of the most stable crystalline form of the compound for which only a single phase solution occurs under equilibrium condition. The term *apparent solubility* refers to the more loosely defined limit of solubility experimentally reached when starting with an amorphous – unstable – solid form of the compound.

Take, for example, the case of indomethacine, whose solubility of the different forms has been reported in several publications [1, 5]. Figure 1.17 allows us to compare the *in vitro* experimental aqueous solubility profiles (measured at room temperature) of the most stable crystalline form γ and of the amorphous form obtained by quench-cooling of the melt. The enhanced solubility of the amorphous form is clearly demonstrated by the shape of the concentration versus time curve. The latter shows a peak of high concentration ("spring effect"), which occurs within the first 20 min. It corresponds to an apparent solubility enhancement ratio of ~5 with respect to that of the crystalline form. The peak then declines to reach a regime of very slow decrease ("parachute effect"), during

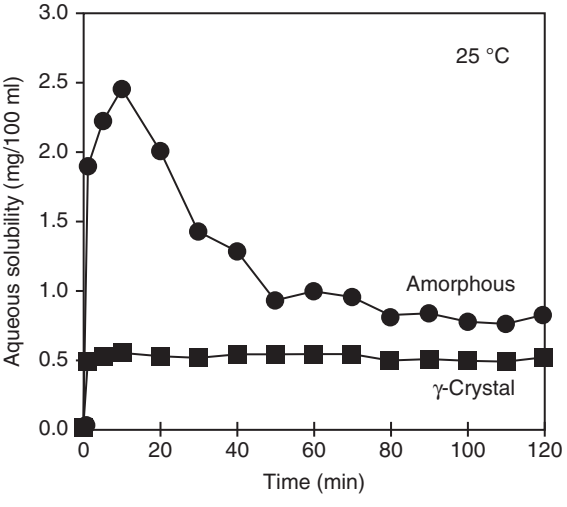

Figure 1.17 *In vitro* experimental aqueous solubility profiles of indomethacin (measured at room temperature). Comparison of the behaviors of the most stable crystalline form γ and of the amorphous form obtained by quench-cooling of the melt (Adapted from Hancock *et al.* [5]. Reproduced with permission of Springer). Similar results are reported in reference [1] figure 4.

which the concentration remains significantly higher than while the dissolution of the crystal form. The ratio of concentration values is still ~1.6 after 2 h. The "spring and parachute" effect is typical of the dissolution profiles found for the amorphous forms of many APIs. The significance of these results to the behavior of pharmaceutical dosage forms is clear. Even if the *in vivo* dissolution kinetics is more complex, it is likely that this type of behavior is able to deliver higher drug concentration for several hours.

It was mentioned in [1] that the presence of crystals could not be detected during the early "spring" stage. However, X-ray diffraction revealed a partial conversion to the crystalline form after 2 h of the "parachute" regime. That is a factor that contributes to the reduction of the ratio of concentration values. These results thus reveal the potential interest in using the amorphous forms, but at the same time helps us to imagine the complexity of the dissolution process – more properly the dilution process – of the nonequilibrium amorphous solid forms. This complexity results from the combination of modified supersaturations, kinetics of dilution, and recrystallization.

The concept of solubility limit itself is different for crystalline and amorphous solid states. This is because the dissolution of a crystal, unlike an amorphous solid, needs to provide the energy, which destroys the crystal lattice. To realize that, it has to be remembered that melting of a crystal is a first-order transition, which also involves a latent heat of melting to destroy the lattice symmetry. On the contrary, "glass melting" is a continuous process in which the viscosity decreases gradually when the temperature increases without requiring the important intake of heat. An amorphous solid is a liquid of extremely high viscosity. There is thus no symmetry-breaking between the amorphous state and the liquid solution state. Therefore, the solubility limit of the amorphous API solute arises from a possible liquid–liquid phase separation. It occurs only if molecules of the solvent and solute "dislike" each other enough ("homo interactions"). For an ideal solution (with supposedly no energy of mixing), there is a limit of solubility for the crystal, since energy is needed to destroy the lattice. On the contrary, there is no solubility limit for the amorphous solid state since a random mixing of the two types of molecules is always favored for entropy reasons. This is also the situation experienced in the case of "hetero interactions" between molecules.

In order to clarify this difference and to show the origin of the apparent solubility enhancement of amorphous API, we adopt a thermodynamic approach. We use a graphical description of the binary system API–solvent, which allows us to intuitively visualize the situation and gives a tangible meaning to the equations.

The stability condition specific to multicomponent systems needs evaluating the right Gibbs free energy, which now includes the mixing enthalpy ΔH_{mix} and the mixing entropy ΔS_{mix} as

$$\Delta G_{\text{mix}}(T) = \Delta H_{\text{mix}} - T\Delta S_{\text{mix}} \tag{1.19}$$

where ΔH_{mix} and ΔS_{mix} are, respectively, the differences between the enthalpy and entropy between the mixed and unmixed states. $\Delta S_{\text{mix}} > 0$, while ΔH_{mix} can be of either sign according to the type of interaction.

It also implies the evaluation of the partial molar Gibbs free energy (the chemical potential μ_i) of each component as

$$G = \mu_A X_A + \mu_B X_B \tag{1.20}$$

for a binary system A (solvant) – B (API), where X_A and X_B are the mole fractions of A and B. Obviously, $X_A = (1 - X_B)$.

It is the equality between the chemical potentials of a given component in different phases that determines the chemical equilibrium conditions between these phases. When the free enthalpy curve for a solution, G, is known as a function of X_B, the chemical potentials are obtained by extrapolating the tangent to the $G(X_B)$ curve to the vertical axis. The equilibrium states of a binary system can be obtained from the $G(X_B)$ curves at a given temperature and using the common tangent construction [36, 64]. Figure 1.18a,b shows examples of free energy diagrams and common tangent constructions. The heat of mixing ΔH_{mix} is due to the interaction energies between neighboring molecules; its value also depends on the composition X_B.

We may distinguish two cases:

1. $\Delta H_{mix} \leq 0$. No miscibility gap in the liquid state. It is the case where A (solvent) and B (solute) molecules "like" each other ($\Delta H_{mix} < 0$; exothermic solutions) or are indifferent to each other ($\Delta H_{mix} = 0$; ideal solution). Figure 1.18a shows a schematic free energy diagram for the liquid solution and crystal B phases at a given temperature T_0. In this case, the $G_{sol}(X_B)$ curve for the liquid solution is U-shaped. At low enough temperature, its value for $X_B = 1$ is that for the amorphous state B^{am}. Figure 1.18a also shows the Gibbs free energy curve of the crystalline API (B^{cryst}). It is supposed that the solvent does not dissolve B^{cryst} so that $G_{cryst}(X_B)$ rises rapidly from its minimum at $X_B = 1$. The two different free enthalpy curves are necessary to describe the equilibrium between the crystal form of B and the liquid solution of B in A. The composition of the liquid solution in equilibrium with the crystal B phase is defined by the common tangent to the $G_{sol}(X_B)$ and $G_{cryst}(X_B)$ curves. X_c is the limit of solubility of B^{cryst}. At the opposite, there is no limitation of the mutual solubility between A and B^{am} in the liquid states, since it is not possible to draw a tangent to $G(X_B)$ starting from $G_{Am}(X_B = 1)$. As mentioned above, in this case there is no thermodynamic limit of solubility for the amorphous state of B (B^{am}). Any limitation is only kinetic.

Mathematically, the limit of solubility of B^{cryst} (X_C) is given by

$$\mu_B^{cryst} = \mu_B^{sol}(X_C) \tag{1.21}$$

with

$$\mu_B^{cryst} \cong G_B^{cryst} \text{ and } \mu_B^{sol}(X_C) = G_B^{am} + RT \ln a_B(X_C) \tag{1.22}$$

where a_B is the activity of the component B in the solution. It is also written as $a_B(X_C) = \gamma_C X_C$, where γ_C is the solution activity coefficient, which takes into account the interaction energies; $\gamma = 1$ for an ideal solution.

Equations 1.21 and 1.22 give the limit of solubility of B^{cryst} as

$$\ln X_C = -\left[G_B^{am} - G_B^{cryst}\right]/RT - \ln \gamma_C$$

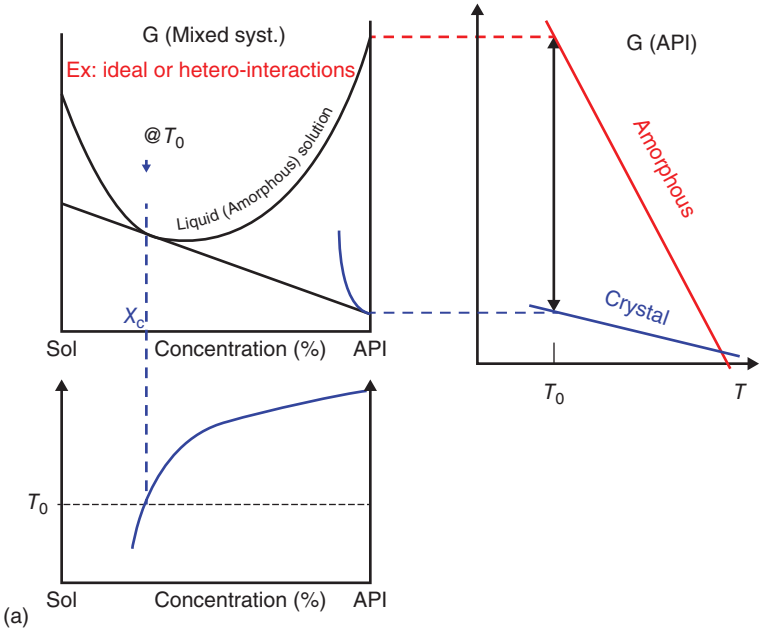
G (Mixed syst.)
Ex: ideal or hetero-interactions
@ T_0
Liquid (Amorphous) solution
X_c
Sol
Concentration (%)
API
T_0
Sol
Concentration (%)
API
G (API)
Amorphous
Crystal
T_0
T

(a)

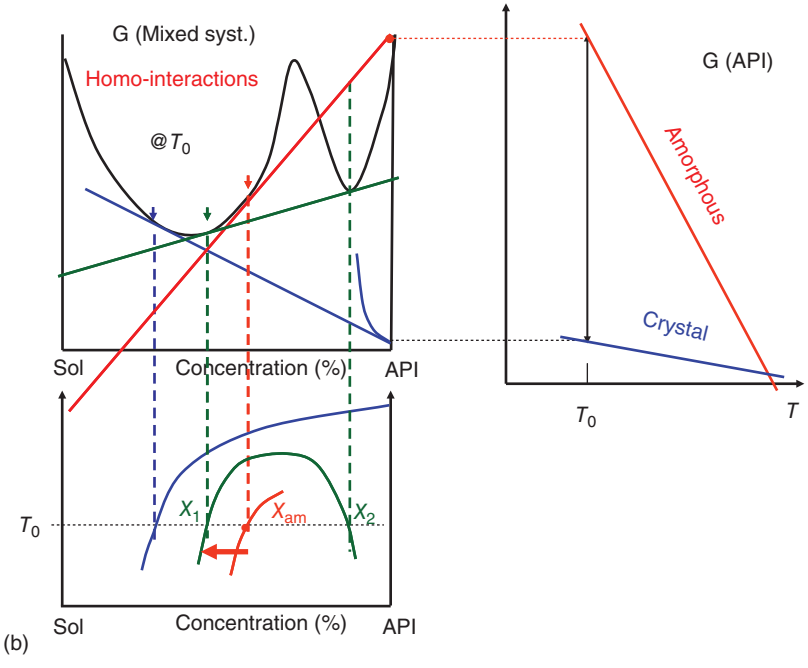
G (Mixed syst.)
Homo-interactions
@ T_0
Sol
Concentration (%)
API
T_0
X_1
X_{am}
X_2
Sol
Concentration (%)
API
G (API)
Amorphous
Crystal
T_0
T

(b)

Figure 1.18 (a) $\Delta H_{mix} \leq 0$. No miscibility gap in the liquid state. Phase diagram and common tangent construction. There is a solubility limit for the crystal state of the API, but not for its amorphous state. (b) $\Delta H_{mix} > 0$. Existence of a miscibility gap in the liquid state (green line). Phase diagram and common tangent construction. The red tangent (and the red curve in the bottom diagram) corresponds to the nonequilibrium situation in which the glassy amorphous state of the API is put in contact with the solvent. The green tangent corresponds to the equilibrated situation: X_1 corresponds to the liquid solution in which the amorphous API dissolves in the liquid solvent. X_2 corresponds to the amorphous solution in which the solvent penetrates into the amorphous API. X_{am} is the initial apparent limit of solubility of the glassy API before penetration of the solvent into it **N.B.** The A and B components in the text correspond respectively to solvent (SOL) and API in the figure.

For an ideal solution, it gives

$$\ln X_C = -[G_B^{am} - G_B^{cryst}]/RT$$

That gives the solubility limit of the crystal, while there is no miscibility gap in the liquid (amorphous) state.

$[G_B^{am} - G_B^{cryst}] = \Delta G(T)$ can be approximately estimated from the heat of melting and melting temperature, as

$$\Delta G(T) \cong \Delta H_m \Delta T / T_m = \Delta H_m (T_m - T)/T_m$$

2. $\Delta H_{mix} > 0$. Existence of a miscibility gap in the liquid state. It is the situation where A and B molecules "dislike" each other. Figure 1.18b shows a schematic free energy diagram for the liquid solution and crystal B phases at a given temperature. Since the amorphous state B^{am} and the liquid solution have the same liquid structure, they lie on the same free energy curve $G_{sol}(X_B)$. At low enough temperature, the $G_{sol}(X_B)$ curve assumes a W-shape with a negative curvature in the middle. This is due to the fact that the enthalpy term is much higher than the entropy term. In that case, the most stable liquid solution is a mixture of two liquid-like phases of different compositions. The compositions of the two phases are given by the common tangent rule, which ensures equilibrium between the chemical entities. These two phases are, respectively, a liquid solution where the amorphous compound B^{am} dissolves in the liquid solvent (concentration X_1) and an amorphous solution where the solvent penetrates into B^{am} (concentration X_2). X_1 is the limit of solubility for B^{am} in the amorphous solid state. As in the previous case, the composition of the liquid solid solution in equilibrium with B^{cryst} phase is defined by the common tangent to the $G_{sol}(X_B)$ and $G_{cryst}(X_B)$ curves. We suppose again that the solvent is insoluble in B^{cryst} The limit of solubility of B^{cryst} is designated by X_C.

The above consideration regarding the solubility limit of the amorphous API is valid for an equilibrium situation. If the penetration of the solvent in the glassy API is slow, the initial value of the solubility limit of the amorphous API (X_{am}) is higher than X_1.

Mathematically, the phase equilibrium between the two liquid phases is such that

$$\mu_B(X_1) = \mu_B(X_2) \tag{1.23}$$

that is,

$$G_B^{am} + RT \ln \gamma_1 X_1 = G_B^{am} + RT \ln \gamma_2 X_2 \tag{1.24}$$

which gives the expression of the limit of solubility X_1 of B^{am}:

$$\ln X_1 = -\ln \gamma_1 + \gamma_2 X_2$$

As above, the limit of solubility X_C of B^{cryst} is given by

$$\ln X_C = -[G_B^{am} - G_B^{cryst}]/RT - \ln \gamma_C$$

If we assume that the activity coefficients at X_C and X_1 are equal, the amorphous and crystal solubility limits are linked by

$$\ln X_1 = \ln X_C + [G_B^{am} - G_B^{cryst}]/RT + \ln \gamma_2 X_2$$

In the above equation, the last term on the right-hand side is the correction associated with the possible absorption of the solvent by the amorphous material.

For the case where $\Delta H_{mix} > 0$, it thus appears that a stable and a metastable limit of solubility are conceivable. The first is related to solubility limit of crystalline B. The metastable limits of solubility X_1 and X_2 are those corresponding to the miscibility gap of the amorphous states when the liquid–liquid phase separation has reached equilibrium. Since the amorphous glassy state is out of equilibrium, the limit of the solubility X_1 depends on its effective level of free energy. It varies with the way of preparing the amorphous state, aging conditions, penetration of water in the glass, and so on.

The considerations given above are to be taken into account in the case of the dissolution in water of a crystalline or amorphous API. They are also to be considered when looking at the dissolution of an API in a polymer excipient [65].

It is important to note that the noncrystalline phase separation associated with a liquid miscibility gap may well be the first stage of a crystallization–devitrification [66]. It is thus important to acquire, as far as possible, a good knowledge of the stable and metastable limits of solubility at all the temperature ranges corresponding to the manufacturing process and drug storage.

1.2 Characteristics of the Disorder in Glass Formers

1.2.1 Glass Formation by Supercooling: Calorimetric Phenomenology

Glass formation (vitrification) is a generic behavior of matter [42, 67–69]. It concerns metals as well as polymers, oxides, or salts. The conventional way to form a glass is by continuous undercooling a liquid below T_m such that crystallization

is avoided. Figure 1.14 shows the route that leads to glass formation in a TTT diagram. It needs to pass quickly the nose of most rapid crystallization at T_n. In so doing, the undercooled liquid is retained in a metastable state with regard to the crystal. Many other amorphization routes can be used for pharmaceutical formulations [70].

A remark, however, is necessary to be made. As shown above, the TTT curve is obtained from experimental determination of the kinetics of recrystallization. It thus results from a combination of nucleation and growth. Passing quickly the TTT nose may certainly avoid experimentally detectable crystallization but it does not necessarily avoid catching some crystalline nuclei that are unable to grow within the amorphous matrix. This is due to the fact that the maxima of nucleation and of growth are separated from each other by temperature. The maximum nucleation rate is situated at a temperature lower than that of the TTT nose. Therefore, it is often observed that recrystallization occurs upon reheating as a result of crystal growth from these nuclei.

Figure 1.19a shows the evolution of C_p for indomethacin upon melting and undercooling. The increase of C_p above melting is due to the dynamic release of the molecular degrees of freedom of large amplitude that characterize the

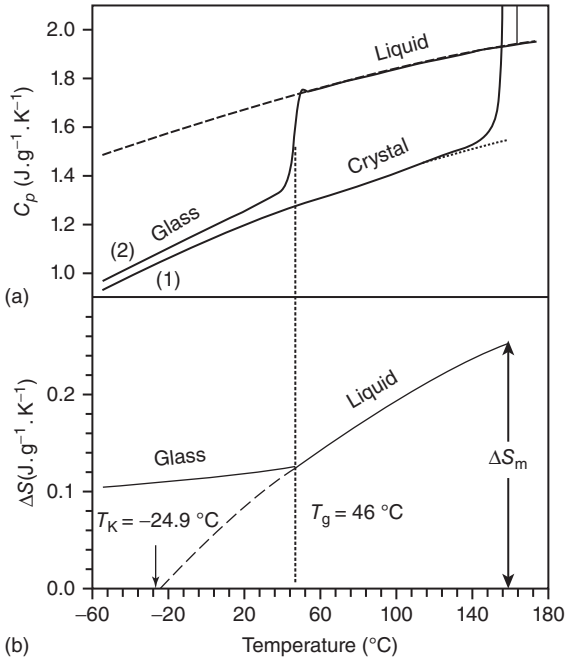

Figure 1.19 (a) Temperature evolution of the specific heat (C_p) of indomethacin in the crystal, liquid, undercooled, and glassy state. The positions of T_m (melting point) and glass transition T_g are shown. (b) Evolution of the excess entropy ($\Delta S = S_{liq} - S_{cry}$) of the supercooled liquid indomethacin in metastable equilibrium relative to the stable crystalline material. $\Delta S(T)$ is obtained by integration of $C_p(T)/T$. ($C_p(T) = T\partial S/\partial T$). It extrapolates to zero at the temperature T_K which is rather close to T_g.

liquid state. By undercooling the liquid rapidly enough (typically 10 °C min^{-1}), crystallization can be avoided. Upon undercooling, C_p keeps a value higher than that of the crystal down to a temperature T_g, at which it decreases continuously (but rather abruptly) to a value comparable (while slightly higher) to that of the crystalline solid. This event defines the *calorimetric glass transition*. It occurs at a temperature (T_g) that is typically around $2T_m/3$ (T_m in kelvin). A dilatometric investigation would also show a drop of the expansion coefficient α_p. The drop of C_p and α_p correspond to a change in the slopes of enthalpy $H(T)$ ($C_p = \partial H/\partial T$) (Figure 1.20), entropy $S(T)$ ($C_p = T\partial S/\partial T$) (Figure 1.19b), and volume $V(T)$ ($\alpha = -[1/V]\ \partial V/\partial T$). T_g marks the transition from the amorphous undercooled liquid to the glassy amorphous state. The value of C_p for a crystal is linked to the vibrational degrees of freedom alone. That suggests that this type of fast motion is also the primary factor contributing to C_p in the glassy state. The much slower and larger relaxational motions, which characterize the liquid state, only contribute for $T > T_g$.

1.2.1.1 The Glass Transition is not a Phase Transition

The glass transition It does not involve any discontinuous structural change, as shown in Figure 1.12. Below T_g, the aspect of the structure factor $S(Q)$, typical of a liquid, is unchanged. The structure essentially remains that of the liquid starting material. The slight shift in the position of the amorphous X-ray bump, which occurs continuously upon cooling, is linked to a progressive contraction.

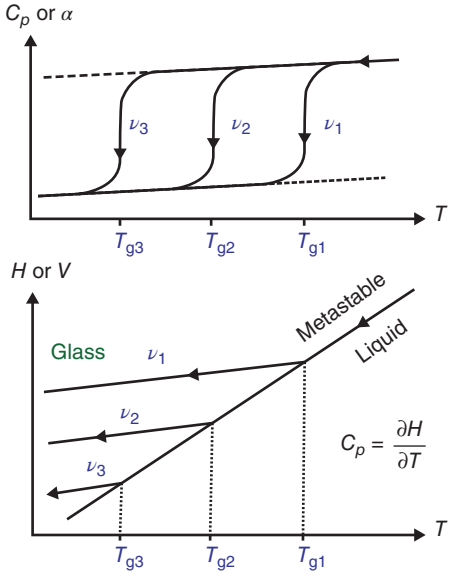

Figure 1.20 Temperature evolution of (C_p, α) for the liquid undercooled at different rates. The corresponding evolution of enthalpy (H) and volume (V). The greater the cooling rate, the higher the value of T_g, and the higher the level of "frozen" H and V.

The change at T_g that can be detected on the structure factor is only the rate of change of this shift with respect to temperature, which slows down below T_g.

1.2.1.2 The Glass Transition is a Kinetic Phenomenon

The vitrification process, in fact, occurs over a temperature interval. Furthermore, the value of T_g depends on the cooling rate. The higher the cooling rate, the higher the value of T_g. Typically, T_g changes by 3–5 °C when the rate changes by one order of magnitude. Figure 1.20 illustrates the evolution of the enthalpy (H) and of C_p as a function of temperature for different cooling rates. Above T_g, the rate of change of enthalpy with respect to temperature is independent of the cooling rate. However, at T_g the slope of $H(T)$ decreases suddenly to a value similar to that of a crystalline solid. Furthermore, enthalpy seems to be frozen at a value which increases with the cooling rate. Similar behavior is found for the entropy $S(T)$ (Figure 1.19b), volume $V(T)$, and so on. Below T_g, the thermodynamic quantities H, S, V, and so on, have values that depend on the way the glass has been formed: they are especially higher as the cooling rate becomes high. Not too far below T_g, slow relaxations of H, V, S, and so on, and the related properties are observed: this is the aging phenomenon by which the glass tries to evolve – on a timescale higher than 100–1000 s – toward the metastable liquid state in internal equilibrium at the temperature of aging. Aging is the manifestation of the glass being in an out-of-equilibrium state. A simple evidence of the nonequilibrium nature of the glassy state is linked to the violation of the Nernst law (third law of thermodynamics, which states that for an equilibrium crystal state at 0 K the entropy should be zero). Because of the break in the evolution of $S(T)$ at T_g, the experimental value of the entropy of a glass at 0 K is positive [71].

In a warm liquid – ordinary liquid – several dynamic processes occur on different timescales. Molecular motions can be roughly divided into two categories: (i) very fast (frequency on the order of terahertz) vibrational and librational motions localized inside the cage formed by neighboring molecules and (ii) the less frequent relaxation processes of diffusion from the cage and molecular rotations of high angles. In glass physics, these processes are named α, β, and so on. The corresponding motions are of a much larger amplitude than that involved in vibrations. They effectively involve a jump over an activation energy barrier. The corresponding frequencies are typically in the gigahertz range at the melting temperature. The two categories of motions contribute to the C_p of an ordinary liquid, while only vibrational motions contribute to the C_p of a crystalline solid. As the temperature of an undercooled liquid decreases, the relaxation time, which is the timescale that characterizes the diffusion processes, becomes longer and longer. T_g is the temperature at which the relaxation time becomes on the order of 100–1000 s, which is the laboratory timescale. At these low temperatures, molecules rearrange so slowly that they cannot explore the entire possible sample configurations in the available time allowed by the cooling rate. The consequence is that slow relaxational motions (the so-called main or α relaxations) no more contribute to the specific heat of the glass below T_g. Only the remaining fast motions may contribute to C_p. For the main part, these are vibrations of molecules.

The slight excess of the specific heat of the glass relative to the crystal seen below T_g (cf. Figure 1.19a) is, in part, due to the fact that vibrations do not take place exactly in the same molecular environment and in part to remaining fast secondary relaxations (β relaxations) [72].

The amplitude of the C_p jump (ΔC_p) at T_g can vary widely according to the compound. The tendency is that liquids with very strong intermolecular (or atomic) bonding generally exhibit small $\Delta C_p(T_g)$ values. Liquids with weak intermolecular bonding (fragile bonding) generally exhibit larger $\Delta C_p(T_g)$ values. As shown for indomethacine in Figure 1.19a, ΔC_p is generally large for molecular materials. According to a terminology proposed by Angell, corresponding glass-forming liquids are called *strong* or *fragile* [4, 73, 74]. It will be shown in the following that these different types of liquids also show differences in the manifestation of their molecular mobility.

As mentioned above, according to the Maxwell relation, the shear viscosity η is proportional to the structural relaxation time (also named the α or the main relaxation process). It is thus equivalent to associating T_g with the temperature at which the viscosity has the value corresponding to a structural relaxation time of 100–1000 s. All glass formers have thus a viscosity of about 10^{13} poises at T_g. Upon cooling, the glass transition occurs when the viscosity of the supercooled liquid becomes so large that molecular motions involved in the viscosity mechanism are arrested on the timescale of the experiment.

1.2.2
T_g as a Transition from an Ergodic to a Non-Ergodic Situation

The differentiation of the states of a system above and below T_g can be depicted schematically in the form of a Gibbs free energy plot (Figure 1.21). Between T_m

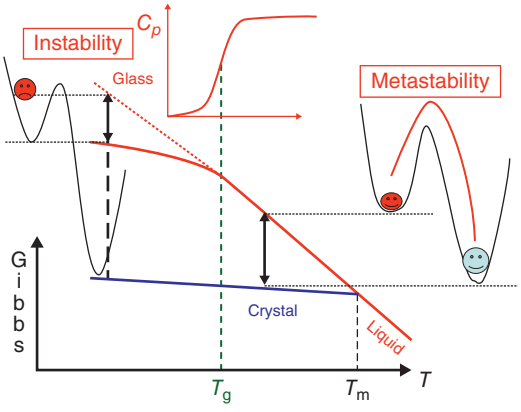

Figure 1.21 Schematic representation of the evolution of the Gibbs function as a function of temperature. Also represented are schematic aspects of the Gibbs function as a function of a configurational variable for two temperatures, respectively, in the domain of the metastable undercooled liquid ($T_g < T < T_m$) and that of the unstable glass ($T < T_g$).

and T_g, the system is metastable but in an equilibrium state. The situation corresponds to the bottom of the free energy well corresponding to the undercooled liquid. Its level is, however, higher than that of the bottom of the well corresponding to the crystal. Below T_g, the system is not even metastable, but it is unstable. Schematically, we can assume its energy position as being frozen somewhere on the side of a potential well, which is not a stable situation. This position depends on the way the glass has been formed. Also, the nonequilibrium system is prone to slow relaxation toward the bottom of a free enthalpy potential well: it is the aging phenomenon [69]. It should, however, be remarked that such a description in term of a well is an oversimplified one. It has never been demonstrated that a unique free energy curve exists out of equilibrium. At equilibrium, what is known is only the existence and position of a potential energy minimum, as well as the curvature of the potential well at that point that determines the responses to a slight perturbation.

Above T_g, the properties can be described with a very limited number of variables (state variables or state functions) energy, specific volume, and so on. This is a consequence of the fact that the motions are extremely fast. The system has enough time to explore all possible molecular configurations. Measured values of the system variables are the results of a good "statistical evaluation" performed by the system itself on all its configurational states. In the language of statistical physics, the system is ergodic because it is equivalent to taking an average over time or over the phase space of the system. On the contrary, in the glassy state it is impossible to describe the properties with such a limited number of variables. Strictly speaking, it would be necessary to know the frozen configurational state of each molecule to describe the glass and its properties. This led to the development of the concept of "potential energy hypersurface" (also known as *energy landscape* [69, 75–77]) on which there are innumerable potential energy minima corresponding to specific molecular configurations of the entire system. For a glass, the experimentally measured physical quantities are the result of an averaging performed on a very limited number of domains of the phase space, that is, of the energy landscape, which is accessible to the system during the measurement. Depending on the way the glass has been formed, the duration on the measurements, the time of the measurement, and so on, different values will be found for the quantities characterizing the system, such as density, optical index, and so on; and this cannot be avoided. It is the reason why patenting the glassy form of an amorphous sample is really a challenging question. In practice, we often try to find at least one additional internal parameter that is able, operationally, to describe the main specific properties. For example, that gave rise to the introduction of the fictive temperature (T_f) concept, to be defined in the following.

1.2.3
The Entropy Below T_g : The Kauzmann Paradox

At the melting temperature, the entropy of a liquid is higher than that of the corresponding crystal. Since C_p ($C_p = T\partial S/\partial T$) of a liquid is higher than that of the

crystal, the entropy (S) of the liquid decreases faster than that of the crystal. For fragile liquids, the entropy difference between the liquid and the crystal decreases by a factor of about 3 between T_m and T_g. For most glass formers, especially for molecular compounds, extrapolating the data obtained above T_g leads to a crossing of the entropy of the liquid with that of the crystal at a positive temperature T_K (the Kauzmann temperature) [78]. Figure 1.19b shows, for instance, the temperature evolution of the excess entropy $\Delta S = S_{liq} - S_{cry}$ for indomethacin. In this case, $T_K \cong -24.9\,^{\circ}C$ (it is located $\approx 173\,^{\circ}C$ below T_m and $\approx 71\,^{\circ}C$ below T_g). If the liquid could be supercooled under equilibrium conditions down to T_K, we would have arrived at the astonishing situation that the liquid (disordered) and the crystal (ordered) would have the same entropy. Figure 1.22 shows some available entropy data plotted by means of a T_m-scaled Kauzmann representation. T_K is all the more close to T_g, so that the rate of change of liquid entropy with respect to temperature is large (more specifically, if the slope at T_m of $\Delta S/\Delta S_m$ with respect to T/T_m (i.e., $\Delta C_p/\Delta S_m$) is larger, and, in any case, larger than 1). From that, it results that most fragile compounds, with high ΔC_p, have their T_K rather close to T_g. The change in slope of S that occurs at T_g, for purely dynamic reasons, permits avoiding this paradoxical situation. If realized, S would become negative when approaching 0 K. That is impossible in the light of the statistical definition of entropy:

$$S(N, E, V) = k_B \ln(\Omega) \tag{1.25}$$

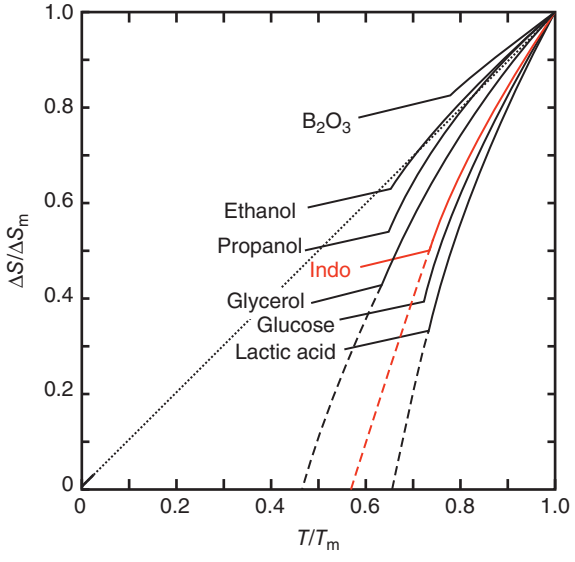

Figure 1.22 Temperature dependence (schematic) of the excess entropy for several supercooled liquids. In red: undercooled liquid indomethacin (data from figure 1.19b) Normalization of ΔS and T have been done against melting values. The temperature T_K, where $\Delta S/\Delta S_m$ extrapolate to zero, depends on the "fragility" of the compound. (Adapted from Kauzmann [78]. Reproduced with permission of American Chemical Society.)

where k_B is the Boltzmann constant and Ω is the number of states accessible to the system of N molecules with fixed energy and volume. Obviously, the minimum value of Ω is 1.

Something should prevent this situation if the equilibrated liquid could be tracked below T_g. Obviously, that is impossible experimentally. The resolution of the Kauzmann paradox is still a matter of theoretical debate. It is, in fact, related to the true thermodynamics of the deeply undercooled liquid state. Several proposals have been made to solve the Kauzmann paradox. It has been suggested that the vanishing of the entropy difference between the liquid and crystal would reveal an ideal glass state only reachable near T_K at infinitely slow cooling. This is the essence of the Adam–Gibbs (AG) approach [79]. The existence of "such a state of high order for the liquid" [78], however, seemed difficult to conceive for Kauzmann himself. He suggested, instead, the existence of an intrinsic limit of metastability of the liquid situated between T_g and T_K. Such a metastability limit (pseudo-spinodal) means that an equilibrated liquid could never be cooled down to T_K because the nucleation barrier opposing crystallization would decrease critically before reaching this temperature. If the glass transition did not occur, the crystallization of the metastable liquid could not then be avoided before reaching T_K. Other works suggest that the extrapolation is no more valid below some temperature higher than T_K and, therefore, the entropy catastrophe at T_K is unphysical [80]. The fact remains that the fast decrease of the entropy of the liquid relative to that of the crystal is one of the most notable aspects of the phenomenology of glass formers. In view of the statistical definition of entropy, it indicates that correlations of a certain type are developing fast in the liquid. However, there is no significant experimental manifestation of ordering in X-ray structural investigations. It is one of the puzzles of glass formation.

1.2.4
Dynamic Features of the Disorder in Glass Formers: The Three Nons. Fragile *versus* Strong Classification

The features of the glass formation and glassy state are not related to the structural ("static") aspects of the compounds but to the distinctive peculiarities of their dynamics. If the nature of the thermodynamic manifestation of the glass transition is well understood, understanding the nature and the temperature evolutions of the relaxation processes while approaching T_g is one of the main challenges in the physics of glasses. Specificities of the dynamics are sometimes referred to as the "three nons" of glass formers [81–83].

- The non-Arrhenius temperature dependence of the relaxation time above T_g
- The non-exponential decay in the response to perturbations from the equilibrium state
- The nonlinearity of the response to thermodynamic perturbations below T_g (The latter is equivalent to saying that the relaxation time is a function of time.).

1.2.4.1 Above Tg: The Dramatic Non-Arrhenius Temperature Dependence of Viscosity and Relaxation Times

Of interest here is the temperature dependence of the viscosity η and of the average relaxation time τ_α. τ_α is the time associated with the so-called main or α relaxation process. It is the characteristic time for the relaxation of some properties (strain, enthalpy, electric polarization, etc.) toward equilibrium after the application of a small perturbation of the intensive conjugate variable (respectively, stress, temperature, electric field, etc.). τ_α can be calculated from the viscosity by means of Maxwell's relation 1.1. It can also be obtained as the inverse mechanical, specific heat, or dielectric loss peak frequency. These definitions of τ_α are not strictly identical, but the differences can be neglected for our purpose. τ_α measures the rate of molecular rearrangements, which involve relatively large rotational and translational molecular displacements over potential energy barriers.

For all normal liquids, under atmospheric pressure, the viscosity η and relaxation time τ_α do not evolve too much between the boiling point and the melting point: η is of order 10^{-2} poise and τ_α is of order of 10^{-12} s. At T_g, after supercooling, η is of the order of 10^{13} poises and τ_α is of the order of 10^3 s. At the glass transition, when the temperature decreased by just about 50% from the boiling point, and about 33% from T_m, η, and τ_α have increased by more than 15 orders of magnitude. It is this spectacular increase at the approach of T_g and the temperature dependence of this increase according to the nature of the glass formers that are challenging.

For oxide glasses (e.g., pure silica) and a few other *strong* liquids (covalent bonds), the temperature evolution of the viscosity η and τ is well represented by an Arrhenius law:

$$\tau_\alpha(T) = \tau_0 \exp E/k_B T \tag{1.26}$$

where the activation energy E is almost constant. It is roughly the energy that is necessary for breaking intermolecular bonds. The prefactor τ_0 is a relaxation time at very high temperature ($\tau_0 \cong 10^{-14}$ s). This expression "predicts" a divergence at 0 K. However, for most liquids – it is the case with most molecular compounds that are rather fragile (weak dispersive chemical bonds) – the evolution of the relaxation while approaching T_g is even more rapid (super-Arrhenius behavior). An attempt to use an Arrhenius description thus requires an activation energy E that is temperature dependent, $E = E(T)$, and strongly increases upon cooling. The effective activation energy $E(T)$ is of the order of $40\,k_B T$ at T_g and increases by a factor of 5–6 between T_m and T_g. In these cases, the activation energy for the structural relaxation is much higher than the bonding energy. Over a rather large temperature range above T_g, (which covers 4–5 order of magnitude in relaxation time), the considerable variation of the viscosity and relaxation times is well described by the Vogel–Fulcher–Tamman (VFT) equation [84]:

$$\tau_\alpha = \tau_0 \exp[DT_0/(T - T_0)] \tag{1.27}$$

where τ_0, D (the "strength" parameter [A]), and $0 < T_0 < T_g$ are adjustable parameters. The VFT equation predicts a virtual divergence at the temperature

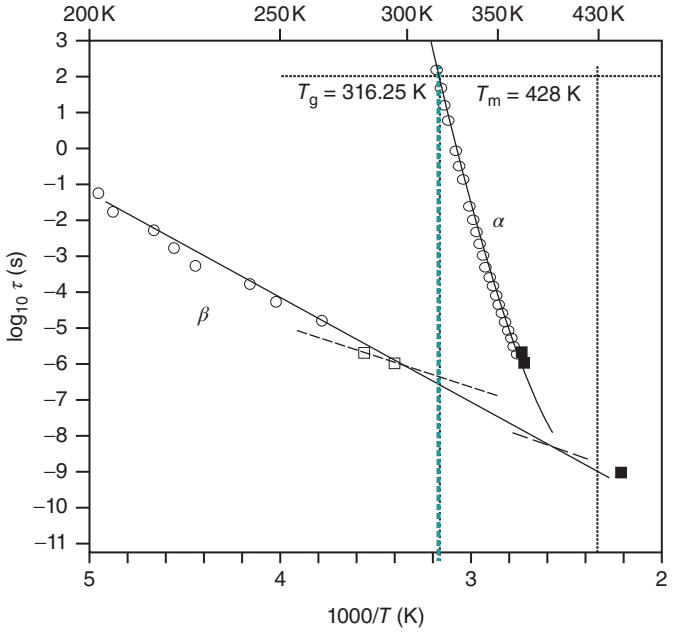

Figure 1.23 Evolution of the main (τ_α) and secondary (τ_β) in the case of amorphous indomethacin. (Adapted from Carpentier *et al.* [85]. Reproduced with permission of American Chemical Society.)

$0\,\mathrm{K} < T_0 < T_g$. For molecular compounds, T_0 is typically a few tens of degrees below T_g. For many systems, T_0 is found to be very close to T_K: typically $0.9 < T_K/T_0 < 1.1$ [69]. Figure 1.23 shows the evolution of τ_α (and an other sub-T_g relaxation to be discussed latter) in the case of amorphous indomethacin [85]. The best fit to the VFT equation is obtained for $\tau_0 = 2.6 \times 10^{-20}$ s, $T_0 = 230.5$ K, and $D = 18.5$. (Similar fitting parameters were found by Paluch *et al.* [86].)

Figure 1.24 shows a T_g-scaled Arrhenius representation, proposed by Angell [67], of viscosity data for a wide variety of glass formers from strong to fragile. This figure illustrates clearly the corresponding change from Arrhenius to super-Arrhenius behavior of relaxational mobilities. In terms of VFT representation, the "strength" parameter D falls between ~3 (fragile) and ∞ (extremely strong). In this plot, the slop at T_g is also a possible measure of fragility. The fragility (or steepness) index m is defined as

$$m = d(\log_{10}\tau_\alpha)/d(T_g/T)(\text{taken at } T = T_g) \tag{1.28}$$

The experimentally observed extreme values are $m = 16$ (strong) and $m = 200$ (very fragile behavior). As has been proposed by Angell [67, 73], glass formers are now classified, in practice, by their more or less non-Arrhenius behavior, that is, by their degree of fragility. For indomethacin, the value of the fragility index was estimated to be $m \approx 79-83$ [85, 86]. This a typical value for a complex "small molecule" compound as found, for example, for salol ($m = 73$) and for nifedipine

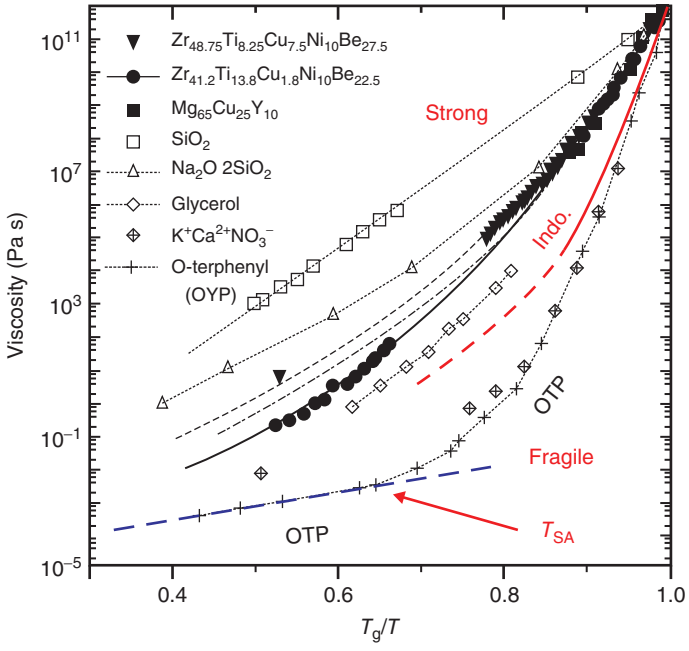

Figure 1.24 T_g-scaled Arrhenius representation, proposed by Angell [71, 83], of viscosity for a wide variety of glass formers from strong to fragile. (Adapted from Busch [87]. Reproduced with permission of Springer.)

($m = 83$). For the rather fragile sorbitol, $m = 93$, while glycerol is found to have an intermediate fragility index (between strong and fragile) $m = 53$. For polymers, the fragility index is generally larger: for polystyrene $m = 139$ and for poly(vinyl chloride) $m = 191$.

Considering that $m = 16$ corresponds to the Arrhenius behavior, D and m are related by [74]

$$m \cong 16 + 590/D \tag{1.29}$$

Another empirical equation was established by Williams, Landel, and Ferry (WLF) [83] to describe the super-Arrhenius relaxation mechanisms in glass-forming liquids. The WLF equation is equivalent to the VFT equation and gives the viscosity as

$$\log \eta/\eta_S = -C_1(T - T_S)/[C_2 + (T - T_S)] \tag{1.30}$$

where η_S is the viscosity at the reference temperature T_S, and C_1 and C_2 are constants. Generally, $T_S = T_g$ is chosen as the reference temperature for convenience. C_1 does not vary so much with the material and has a value of ~16–17, which corresponds to the number of decades of viscosity decrease between T_g and an infinitely high temperature (where $\eta_\infty \approx 10^{-4}$ poise) [88]. On the contrary, C_2 depends on the fragility and thus on the material. The relation between C_2

and the fragility index m is given by

$$m = C_1 \cdot T_g / C_2 \tag{1.31}$$

C_2 is linked to T_g and the VFT temperature T_0 by

$$T_0 = T_g - C_2 \tag{1.32}$$

It is generally observed that both VFT and WLF models are able to describe only the behavior in temperature domain close to T_g.

1.2.4.2 Possible Connection Between Dynamics and Thermodynamics

From what we have seen, a connection between dynamics an thermodynamics seems to be emerging:

- Strong glass formers have a small ΔC_p at T_g and an Arrhenius behavior of relaxations.
- Fragile glass formers generally have large ΔC_p at T_g and a pronounced non-Arrhenius behavior of the relaxations.

Furthermore, the Kauzmann temperature T_K is usually found to be very close to the VFT temperature T_0. This suggests that a structural arrest of configurational rearrangements would occur at T_K if the system could be cooled under equilibrium condition down to that temperature.

Adam and Gibbs [79] developed a theory that rationalizes the relationship between dynamics and thermodynamics. It assumes a phase transition to a state of zero configurational entropy and infinite relaxation time at T_K. This leads to expressing the temperature evolution of the viscosity, or equivalently of the relaxation times, as a function of the configurational entropy S_c:

$$\eta \propto \tau \propto A \exp C/TS_c(T) \tag{1.33}$$

where C is a constant containing an energy barrier term. If it is assumed that structural equilibrium is maintained at all temperatures, the configurational entropy varies with temperature according to the following expression:

$$S_c(T) = \int_{T_K}^{T} (\Delta C_p / T')\, dT' \tag{1.34}$$

where ΔC_p is the configurational specific heat [$\Delta C_p \approx C_p(\text{liquid}) - C_p(\text{crystal})$], and T_K is the temperature at which the configurational entropy is supposed to fall to zero. If we use Eq. (1.33) and the approximation $\Delta C_p = A/T$ (this approximation is usually valid for non-polymeric systems but the result is not very sensitive to the form of ΔC_p), the empirical VFT equation is recovered with $T_0 = T_K$:

$$\eta \propto \tau \propto A \exp[DT/(T - T_K)] \tag{1.35}$$

In the formulation of the AG equation, it is assumed that structural equilibrium is maintained at all temperatures, even below T_g, which is experimentally impossible. The equation is thus strictly applicable only for $T > T_g$. For $T < T_g$, the AG equation is usable only to provide a formal expression that links the virtual critical

slowing down to the thermodynamic pseudo-singularity at T_K. It would make no sense to use the argument that for $T < T_K$ there is no molecular mobility anymore and that amorphous compounds are stable at these low temperatures.

Even if the possible existence of an ideal glass state, having an entropy equal to that of the crystal, remains speculative, the AG expression provides a very good correlation between dynamic and thermodynamic data (for $T > T_g$) for a large majority of compounds. This analogy between the VFT law and AG prediction seems to show that the temperature at which relaxation times tend toward infinite values corresponds to the temperature at which the configurational entropy reduces to zero. It should be noted, however, that the experimentally measured excess heat capacity may include some vibrational contributions in addition to purely configurational ones. That may induce some uncertainty in the evaluation of T_K and be a source of slight discrepancy between T_0 and T_K.

AG envisaged the idea of cooperatively rearranging regions (CRRs), whose size increases as the temperature decreases [89]. As a consequence, their number decreases, which reduces the number of effective configurational degrees of freedom and therefore the configurational entropy. The AG theory predicts that the minimum size of CRRs of molecules is inversely proportional to S_c. This size would be in the nanometer scale near T_g. One picture is that the CRR blocks would virtually become of infinite size at T_K as well as the characteristic time required to cause a transition from one configuration to another. However, the nature of these CRRs, their possible interactions, and so on, remain poorly understood [90] as well as their real involvement in the dynamics of glass formers [68].

1.2.4.3 Above Tg: Non-Exponential Relaxations and Dynamic Heterogeneity

For ordinary "warm" liquids, the relaxation toward equilibrium of any microscopic or macroscopic property $f(t)$, after a small applied perturbation, can be usually described by an exponential time decrease. The relaxation function $f(t)$ measures, for example, the instantaneous polarization following a step change of the electric field. On the other hand, for a supercooled liquid, the response $f(t)$ is no longer exponential. It has a sluggish behavior, which contrasts with the behavior above T_m. At long enough times, which correspond to that of the α relaxation process, it may be generally expressed with the Kohlraush – Williams – Watts function [91] or the "stretched exponential":

$$f(t) \propto \exp[-(t/\tau)^{\beta}] \tag{1.36}$$

where the value of the parameter β is between 0 and 1. The exponential, the so-called Debye behavior, is recovered for $\beta = 1$. The smaller the value of β, the more stretched the relaxation. The stretching generally increases when temperature decreases and reaches values on the order of 0.3 – 0.8 at T_g. It was observed [92, 93] that low values of β are generally correlated with a high fragility index m.

Non-exponential relaxation described by Eq. (1.36) can be interpreted in terms of a superposition of exponential function with a distribution of relaxation times. It is (was) a matter of considerable interest to know whether this non-exponential

nature is intrinsic or whether it is the result of a spatial heterogeneity [94]. A number of experiments have shown the existence of kinetic heterogeneities in glass-forming systems with regions of slower and faster molecular mobility. The size of these heterogeneities is estimated to be of some nanometers at T_g. It must be mentioned that these heterogeneities are purely dynamic in nature. As to whether these dynamic heterogeneities may have some structural connection remains a challenging issue.

Ngai proposed a coupling model [92, 95] according to which the primitive relaxation is exponential – $\exp(t/\tau_0)$ – for $t < t_c$. τ_0 is the "uncoupled" relaxation time. For $t > t_c$, molecules move cooperatively and the relaxation becomes stretched and fittable with $\exp[-(t/\tau)^{\beta}]$. For usual glass formers, the crossover time $t_c \approx 2$ ps. The fractional exponent coupling parameter $n = 1 - \beta$ is a measure of the strength of the intermolecular cooperativity. This formalism allows us to derive a simple relation between $\tau(T)$, $\tau_0(T)$, β, and t_c. This relation is operationally useful to identify the secondary β relaxation since $\tau_0(T)$ is supposed to be "close" to $\tau_\beta(T)$ (see below).

Some experimental methods can characterize directly the relaxation in the time domain [96]. However, the dynamic response of a system can also be analyzed in the frequency (ω) domain by applying a sinusoidal perturbation. What is measured in that case is a frequency-dependent complex susceptibility $\chi^*(\omega)$. The imaginary part (loss spectrum) $\chi''(\omega)$ is the Fourier transform of $df(t)/dt$, where $f(t)$ is the corresponding relaxation function. A relaxation is highlighted by a peak in the $\chi''(\omega)$ spectrum, with a maximum for the characteristic frequency $\omega_c \propto 1/\tau$. Figure 1.25 shows the $\chi''(\omega)$ spectra for the α relaxation of amorphous indomethacin measured at different temperatures and plotted as a function of $\log_{10}(\omega)$. When the temperature decreases, the peak shifts toward low frequencies (i.e., large relaxation times). The width of the peak gives information on the departure from pure Debye behavior. The broadening of the peak observed at low temperature reflects the stretching of the relaxation function mentioned above.

1.2.4.4 *Below T_g: Aging, Nonlinearity, Secondary Relaxations*

Aging and Variability of Glass Structure

When a liquid is undercooled and crystallization is avoided, a temperature ($\approx T_g$) is finally reached where cooling is too fast for the molecules to arrange into an equilibrated state. The liquid "falls out of thermal equilibrium." The liquid structure nearly freezes. As a consequence, below T_g, the sample is in a structural state corresponding to a higher temperature. The faster the cooling rate, the higher will be this temperature. The glassy state thus depends markedly on the cooling conditions in relation to the relaxational properties of the liquid. Practically all physical properties of a glass are modified to some extent if the conditions of the cooling process are varied. Other consequences of the nonequilibrium state of the glass are a variety of phenomena such as aging, memory effect, or rejuvenation [97]. Indeed, we must understand that, even though slow, the molecular mobility still remains. It provides the mechanism by which the glassy compound slowly evolves

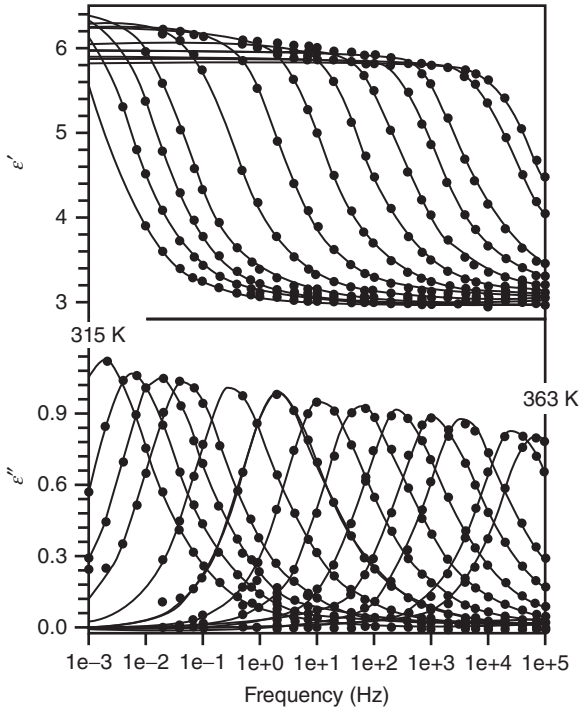

Figure 1.25 Real and imaginary parts of the dielectric susceptibility of amorphous indomethacin at different temperatures between 315 and 363 K. Solid lines are a fit with a Havriliak–Negami function. (Adapted from Carpentier *et al.* [85]. Reproduced with permission of American Chemical Society.)

with time or ages. Therefore, for identically prepared glasses, the larger the deviation from T_g, the slower the aging.

Upon aging, the volume of the glassy material changes with time. Similarly, an evolution of enthalpy will also take place. DSC is a common method to characterize this enthalpy evolution. The result of such an experiment is depicted in Figure 1.26 for amorphous indomethacin in which two different aging temperatures T_a (20 and 35 °C) were imposed. In these experiments, the sample is first melted ($T > T_m \approx 161$ °C) and then cooled (at 10 K min^{-1}) to a temperature $T_a < T_g$, where it is aged for a time t_a. The heat flow corresponding to each value pair (T_a, t_a) is then measured upon reheating. For each T_a, the experiment is repeated for different values of t_a. The main pieces of information provided by these curves are the following: (i) An overshoot appears and grows as t_a increases; (ii) The rate of increase of the overshoot is faster for higher aging temperature. For $T_a = 35$ °C, a saturation is nearly reached at $t_a = 1$ h ($\approx T_g - 8$ °C); (iii) For $T_a = 20$ °C, the overshoot grows more slowly but reaches higher values; (iv) The stronger growth of the overshoot for $T_a = 20$ °C is correlated to a shift toward higher temperatures, which gives rise to an apparent increase of T_g.

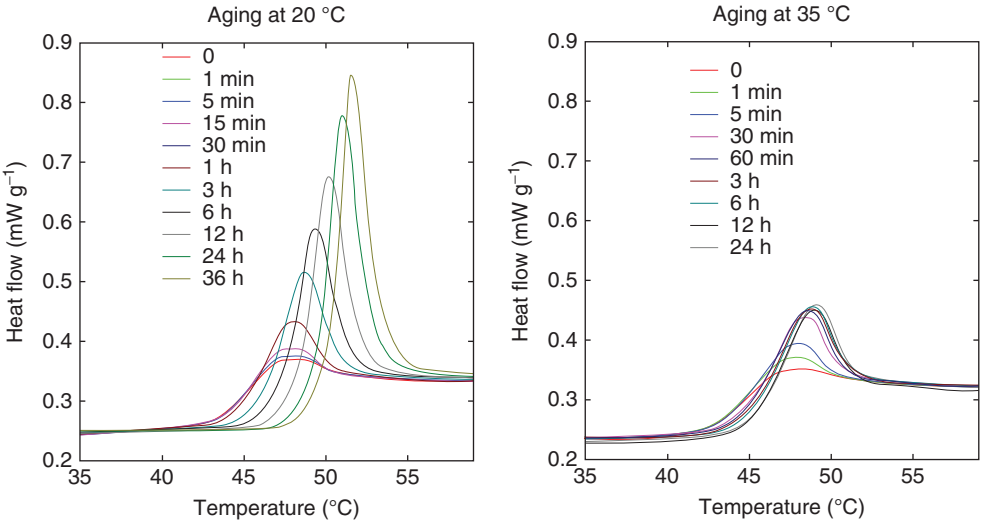

Figure 1.26 DSC heating scans for amorphous indomethacin aged during various times t_a at two different temperatures (20 and 35 °C).

The heat flow response is related to the heat capacity, which is the temperature derivative of enthalpy. Consequently, an overshoot reflects a fast transient evolution of enthalpy as illustrated in figure 1.27. During annealing, the glass relaxes slowly toward metastable equilibrium and loses. When heated through the glass transition temperature, the lost enthalpy is recovered rapidly, and gives the overshoot. Enthalpy recovers the supercooled metastable liquid value upon heating at the temperature where molecular mobility is high enough to allow this. At low aging temperatures, molecular mobility is very slow and the structural relaxation process is kinetically limited. However, the enthalpy difference between the nonequilibrium glass and the equilibrium supercooled metastable liquid is large (see for example figure 1.20). The glass relaxes more slowly but may reach low enthalpy values. As a result the recovery may give rise to a large overshoot after long enough aging. When T_a is close to T_g, the glass nearly reaches equilibrium during a rather short annealing, but the energy loss is small and so is the size of the overshoot. The progressive shift of the overshoot toward higher temperatures is an indication that annealed glasses have less molecular mobility compared to unannealed glasses. This is due to the fact that part of the residual enthalpy and free volume are lost upon annealing. The resulting lesser mobility delays the recovery upon heating. That the molecular mobility, which allows structural relaxation, is decreasing as the structural relaxation progress expresses the nonlinearity of the phenomenon.

Fictive Temperature

While a glass is a non-ergodic state that cannot be described by state functions, its properties and structural relaxation are often tentatively described in terms

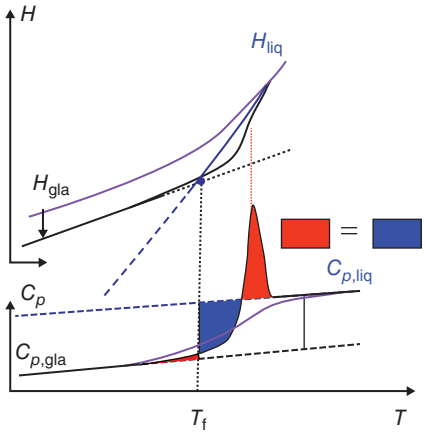

Figure 1.27 Fictive temperature. (Top) Definition on the $H(T)$ curve. It shows how T_f decreases when the glass is annealed. (Bottom) Experimental determination of T_f by application of an "equal area rule" on $C_p(T)$ curve.

of the change in the fictive temperature T_f. The notion of a fictive temperature T_f was formulated by Tool [98]. T_f of a nonequilibrium glassy system is defined as the actual temperature of the same compound in the equilibrium, metastable, undercooled state whose structure is expected to be similar to that of the nonequilibrium compound. The definition is illustrated in Figure 1.27, which also shows a method ("equal area rule") to determine T_f for a glassy compound using experimental values of a property of this compound (e.g., C_p) when the temperature evolutions of this property for the liquid (C_p^l) and glassy (C_p^g) states are known. From this picture, we can see that there is a one-to-one correspondence between the enthalpy level of the glass and its fictive temperature. Upon aging, H and T_f decrease together. H tends to reach the equilibrium metastable level at the same time as T_f tends to reach the actual aging temperature T (at equilibrium $T_f = T$, which is always the case for $T > T_g$).

Nonlinearity

It has long been experimentally observed that below T_g, the shear viscosity depends on the degree of structural relaxation [68, 99]. As a result of the Maxwell relation 1.1 between the shear viscosity η_s and the shear stress relaxation time τ_s ($\eta_s = G_\infty \tau_s$), another way of saying the same thing is that the relaxation time, that is, the rate of structural relaxation, is itself dependent on the progression of the relaxation process. This is basically due to the fact that the relaxation time τ_s depends on the enthalpy and free volume values, which decrease upon annealing at a rate that is determined by τ_s. If the nonequilibrium state of the glass is approximately characterized by a fictive temperature alone, this is reflected in the fact that τ depends on the fictive temperature T_f in addition to the ambient temperature T [81].

To summarize, at a given temperature T below T_g, the instantaneous values of H and V (depicted by T_f) determine the mobility (τ), while τ determines the

rate dT_f/dt at which T_f (and therefore H, V, etc.) changes. Aging can thus be understood via following the closed-loop scheme [100]:

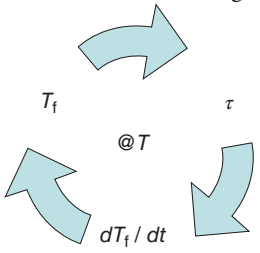

The following TNM (Tool–Narayaswamy–Moynihan) expression [101] is commonly used to describe the dependence of τ on both T and T_f:

$$\tau(T, T_f) = \tau_0 \exp[\, xA/(k_B T) + (1 - x)A/(k_B T_f)] \tag{1.37}$$

where x is the nonlinearity parameter ($0 \leq x \leq 1$). The maximum nonlinearity is for $x = 0$. The first term in the bracket expresses the effect of temperature, and the second term expresses that of the fictive temperature [102]. This description is highly empirical.

Another equation adapted from the more physical AG model and the entropy evolution (referred to as AGF: Adam–Gibbs–Fulcher [103–105]) has been proposed to express the time dependence of τ in terms of T_f evolution. The generalization of the AG equation allows us to describe the mobility both above and below T_g for a real system. It is obtained by expressing the configurational entropy S_c as a function of T_f rather than T.

$$\tau(T, T_f) = A \exp[C/TS_c(T_f)] \tag{1.38}$$

For $T > T_g$, the system is in a state of equilibrium and $T_f = T$, and Eq. (1.33) is recovered.

For $T < T_g$, in the fictive temperature formalism, the configurational entropy of the nonequilibrium system (the glass) at temperature T ($S_c^g(T)$) is taken to be identical to the configurational entropy of the equilibrium supercooled system at T_f ($S_c{}^{eq}(T_f)$).

$$S_c^g(T) = S_c^{eq}(T_f) = \int_{T_K}^{T_f} (\Delta C_p/T')\, dT' \tag{1.39}$$

where ΔC_p is the extrapolated value of the configurational heat capacity of the equilibrium supercooled system. Substitution of Eq. (1.39) (rather than Eq. (1.33)) in Eq. (1.38) gives the AGF equation for the relaxation time:

$$\tau(T, T_f) = \tau_0 \exp[\, E/T(1 - T_0/T_f)] \tag{1.40}$$

and thus allows us to define an isostructural activation energy

$$E(T_f) = E/(1 - T_0/T_f) \tag{1.41}$$

Since $T \leq T_f$, $E(T_f)$ is lower than the equilibrated value of the activation energy $E(T)$. Aging induces a slow decrease of T_f, which moves toward the aging temperature T. Aging thus induces an increase of $E(T_f)$, which slowly tends to be closer

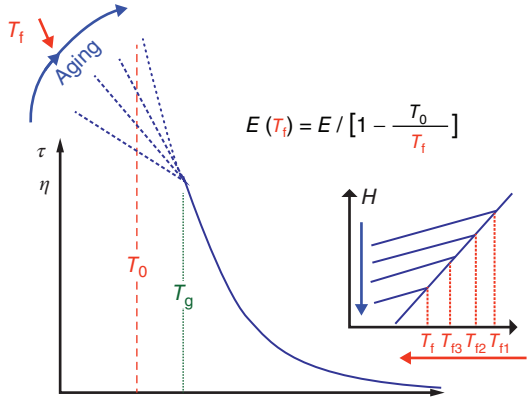

Figure 1.28 Evolution of the apparent activation energy upon aging the glass. Correlation with the evolution of the fictive temperature T_f is underlined.

to the equilibrated value $E(T)$. The evolution of the relaxation times corresponding to the forgoing description is depicted in Figure 1.28. The change of slope at T_g is related to the evolution of the measured configurational entropy.

Combination of the AGF and NMN equations allows us to express the nonlinearity factor $x \approx 1 - T_K/T_g$. This relation and that linking m to β [92] show that the levels of fragility, non-exponentiality, and nonlinearity are connected and rise together. When comparing different glass formers, the tendency is as follows:

x decreases when m increases, β decreases, and T_K increases toward T_g.

To obtain an accurate – albeit phenomenological – description of relaxation features and evolution of the specific heat as a function of the temperature upon cooling and heating through the glass transition, it is necessary to combine a stretched exponential expression of the relaxation function with the T_f-dependent expression of the relaxation time $\tau(T, T_f)$ [103, 106].

Secondary Relaxations

Below Tg, not all molecular mobility ceases to occur. In addition to the fast vibrational motions of atoms or molecules, and the very slow relaxations associated with the irreversible aging of glasses (main or α process), there are small-scale molecular motions that can be detected generally by dielectric (see the chapter by Paluch *et al.* in this book) and mechanical relaxation studies. The timescale of these secondary relaxation processes is generally several orders of magnitude lower than that of the main relaxation motions. Some of these motions can be attributed to the internal degrees of freedom of the molecules when the latter are flexible. However, there can exist other types of secondary relaxation processes, which have been identified for the first time by Johari and Goldstein [107]. These relaxations can be observed even for rigid molecular substances and are thus an intrinsic property of amorphous systems. They are named Johari–Goldstein (JG) β processes (β_{JG}), or simply β processes. The other types of secondary processes are often designated by other greek letters γ, δ, and so on.

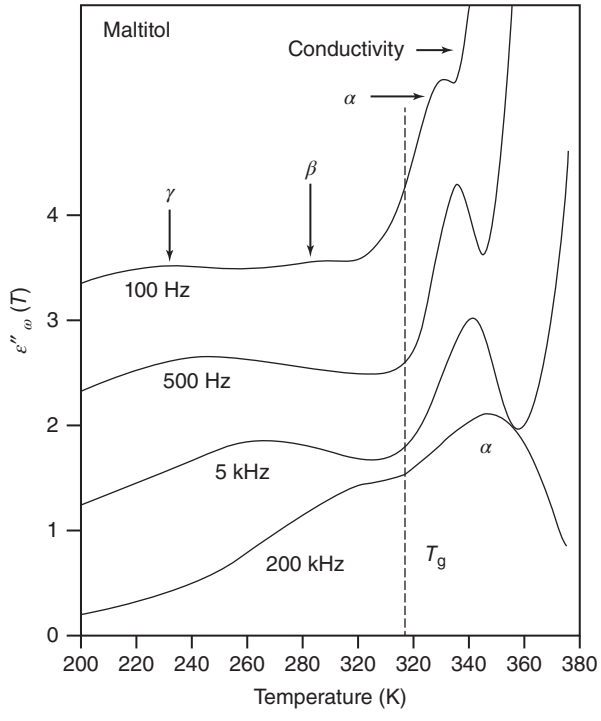

Figure 1.29 Isochronal imaginary part of the dielectric response of amorphous maltitol plotted against the temperature for four typical frequencies. (Adapted from Carpentier and Descamps [108]. Reproduced with permission of American Chemical Society.)

Figure 1.29 shows the dielectric loss factor of amorphous maltitol as a function of temperature for several frequencies [108]. The main (α) and secondary relaxations are seen for temperatures, respectively, above and below T_g. Below T_g, for a frequency = 100 Hz, two secondary processes are visible. It is sometimes difficult to distinguish JG β processes from other secondary processes. This aspect is discussed in [109]. In the case of maltitol, the JG β process is most probably that observed at the highest temperature. The other one (γ) is associated with faster intramolecular motions. This latter mode is also observed in sorbitol [108]. The relaxation map shown in Figure 1.30 summarizes the temperature evolution of the mean relaxation times of maltitol corresponding to the different modes of relaxation. The secondary relaxation processes may persist above T_g. α and β processes show a tendency to merge above T_g (see Figures 1.23 and 1.30). Secondary relaxations are more easily observed below T_g, where they have an Arrhenius type evolution with activation energies much lower than that of the α process. For all these aspects, see the chapter by Paluch *et al.*

There is general agreement that the β_{JG} relaxation involves localized molecular motions as opposed to α-type motions that are linked to cooperative rearrangements. However, the nature of theses motions and there spatial distribution are

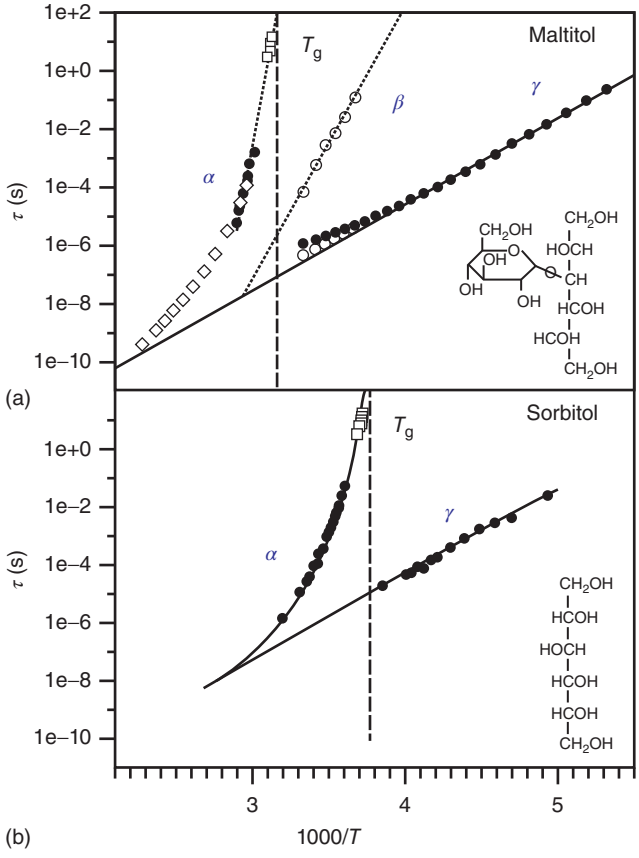

Figure 1.30 Arrhenius plot summarizing the temperature evolutions of the relaxation times of (a) amorphous maltitol and (b) amorphous sorbitol. (Adapted fromCarpentier and Descamps [108]. Reproduced with permission of American Chemical Society.)

still matters of debate. There are two main types of interpretation. The first is that of Johari [110], which considers that the glass is structurally nonuniform. β relaxation would correspond to motions of molecules situated at local regions of low density, the so-called *islands of mobility*. Another interpretation [111] considers that the main and secondary relaxations are continuous and represent the evolution with time of a single process whose long-time behavior corresponds to the main process. The model of Ngai has some connection with the latter model. Ngai proposed that the primitive relaxation of his coupling model is approximately located near the most probable relaxation time τ_β of the JG relaxation since both relaxations are noncooperative in nature [95]. The long-time behavior (α process) would correspond to the motions of molecules moving cooperatively.

The irreversible decrease in enthalpy and volume due to physical aging brings about a decrease of the height of the JG β relaxation peak. That is interpreted by Johari as being the result of a decrease in the number of molecules involved in the

islands of mobility. It is easy to imagine that aged glasses require more cooperativity for structural relaxation because the packing is denser.

1.2.5 Fragility and Polyamorphism in the Energy Landscape View Point

1.2.5.1 Fragility and Landscape Topology View Point

Goldstein [112], more than 45 years ago, already pointed out the existence of the crossover temperature (such as T_{SA} in Figure 1.24) that occurs well above T_g in the moderately undercooled liquid state. He proposed that for $T < T_{SA}$, the dynamics corresponding to the slow α process is dominated by thermally activated relaxation processes over potential energy barriers that are larger than the typical thermal energy ($k_B T$). This relates to the energy landscape view point and its topology (Figure 1.31). From this view point, the dramatic slowing down of relaxations

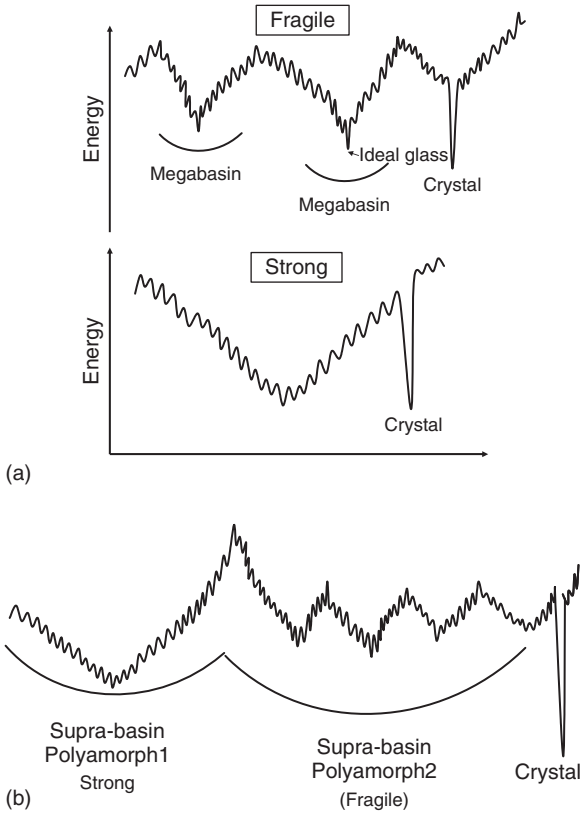

Figure 1.31 Examples of energy landscape topologies. (a) Difference between strong and fragile glass formers. In the latter case, "megabasins" are separated by relatively high barriers. Smaller basins inside "megabasins" could be linked to β relaxations. (b) Example of polyamorphism. Each polyamorph has its proper "supra-bassin".

at low T – which is typical of fragile glass formers – is linked to the increasing difficulty for the amorphous system to find new minima in the landscape. Fragile behavior is thus linked to a specific landscape topology with "megabasins" linked by relatively high energy barriers. Moving from one "megabasin" to another one involves a high energy activation (much larger than the energy involved in individual bonding energy between molecules) and cooperative rearrangement of many molecules (similar idea as that of CRR). In this case, the slowing down of α relaxations is associated with the fast decrease of the configurational entropy, which measures the number of minima that are available at any given temperature. These minima become increasingly hard to find for the amorphous system when the temperature decreases. It has been suggested that the faster, well-separated β relaxations would be linked to the elementary relaxations between small, contiguous basins that decorate the interior of a "megabasin" [69, 113]. On the contrary, strong formers could be associated to a single "megabasin" with a multitude of "small" barriers inside, which have roughly the activation energy corresponding to the breaking of the bonds between individual molecular entities. Figure 1.31a shows a schematic representation of the different types of landscape topologies.

1.2.5.2 Polyamorphism and Landscape Topology

The concept of polyamorphism has become very popular for a while both in the field of fundamental physics and pharmaceutical science. In the latter case, it is because it is well established that the properties of amorphous glasses, which can impact pharmaceutical behavior, can be different according to the previous history of the formulation and (or) the time of storage. As mentioned above, the primary reason for such a variability is linked to the non-ergodicity of the glassy state for the same compound. There is thus some kind of unavoidable "multiamorphicity" of a glass connected, for example, to a variable fictive temperature. It reflects the landscape localization of the frozen molecular configuration and the limited extension of this landscape that is accessible during experimental times. In contrast to this behavior, a truly polyamorphic situation for a compound implies the existence of two different liquid structures for the same material. This may lead to a possible liquid/liquid phase transition and existence of an interface between these phases. The polyamorphism of water is certainly the most widely studied example [71, 114, 115]. There are a few documented examples of suspected polyamorphism for organic and pharmaceutical compounds (for a discussion see [116]). The experimental identification of a true polyamorphism in such compounds is very difficult. From this perspective, the case of the "glacial phase" of triphenyl phosphite (TPP) is particularly illustrative. Indeed, there is a danger of confusion with the existence of a mesophase [117], or a situation of a fully nanocrystallized liquid [118, 119]. A situation of polyamorphism can be described by a potential energy hypersurface with "supra-basins" corresponding to the specific physical properties of the different polyamorphic varieties. Figure 1.31b gives a schematic representation of this landscape. One "polyamorph" may be strong, while the other is fragile. In connection with the situation of amorphous ice, Angell [71] has suggested that

"polyamorphs" may indeed differ in their strength: a low-density form acting as a strong glass former, while a high-density form as a fragile glass former.

Acknowledgments

The authors thank their colleagues F. Affouard, E. Dudognon, N. Correia, L. Carpentier, F. Danède, P. Derollez, A. Hedoux, Y. Guinet, and L. Paccou for their kind cooperation and interaction. This work was funded by the EU INTERREG IV A 2 Mers-Seas-Zeeën Crossborder Cooperation Programme (IDEA and AMPTECH).

References

1. Murdande, S.B., Pikal, M.J., Shanker, R.M., and Bogner, R.H. (2010) Solubility advantage of amorphous pharmaceuticals: I. A thermodynamic analysis. *J. Pharm. Sci.*, **99** (3), 1254–1264.
2. Craig, D.Q.M., Royall, P.G., Kett, V.L., and Hopton, M.L. (1999) The relevance of the amorphous state to pharmaceutical dosage forms: glassy drugs and freeze dried systems. *Int. J. Pharm.*, **179**, 179.
3. Yu, L. (2001) Amorphous pharmaceutical solids: preparation, characterization and stabilization. *Adv. Drug Delivery Rev.*, **48**, 27.
4. Hancock, B.C. and Zografi, G. (1997) Characteristics and significance of the amorphous state in pharmaceutical systems. *J. Pharm. Sci.*, **86**, 1.
5. Hancock, B.C. and Parks, M. (2000) What is the true solubility advantage for amorphous pharmaceuticals? *Pharm. Res.*, **17**, 397.
6. Baird, J.A. and Taylor, L.S. (2012) Evaluation of amorphous solid dispersion properties using thermal analysis techniques. *Adv. Drug Delivery Rev.*, **64**, 396.
7. Graeser, K.A., Patterson, J.E., and Rades, T. (2008) Physical stability of amorphous drugs: evaluation of thermodynamic and kinetic parameters. *J. Pharm. Pharmacol.*, **60**, 116.
8. Bhattacharya, S. and Suryanarayanan, R. (2009) Local mobility in amorphous pharmaceuticals-characterization and implications on stability. *J. Pharm. Sci.*, **98**, 2935.
9. Paudel, A., Geppi, M., and Van Den Mooter, G. (2014) Structural and dynamic properties of amorphous solid dispersions: the role of solid-state nuclear magnetic resonance spectroscopy and relaxometry. *J. Pharm. Sci.*, **103**, 2635.
10. Massey, B.S. and Ward-Smith, J. (1998) *Mechanics of Fluids*, 7th edn, Taylor & Francis.
11. Dyre, J.C., Christensen, T., and Olsen, N.B. (2006) Elastic models for the non-Arrhenius viscosity of glass-forming liquids. *J. Non-Cryst. Solids*, **352**, 4635.
12. Warren, B.E. (1970) *X-Ray Diffraction*, Addison-Wesley, New York.
13. Guinier, A. (1994) *X-Ray Diffraction in Crystals, Imperfect Crystals, and Amorphous Bodies*, Dover Publications.
14. Guinier, A. (1964) *Théorie et technique de la radiocristallographie*, Dunod, Paris.
15. Billinge, S. and Thorpe, F. (1998) *Local Structure from Diffraction*, Springer, New York: Plenum Press.
16. Hosemann, R. (1950) Der ideale Parakristall und die von ihm gestreute kohärente Röntgenstrahlung. *Z. Angew. Phys.*, **128**, 465.
17. Elliott, S.R. (1990) *Physics of Amorphous Materials*, Longman Scientific & Technical.
18. Sherwood, J.N. (1979) *The Plastically Crystalline State*, John Wiley & Sons,

Ltd., Chichester, New York, Brisban, Toronto.

19. Suga, H. and Seki, S. (1974) Thermodynamic investigation on glassy states of pure simple compounds. *J. Non Cryst. Solids*, **16**, 171.
20. Descamps, M., Caucheteux, C., Odou, G., and Sauvajol, J.L. (1984) Local molecular order in the glassy crystalline phase of cyanoadamantane: diffuse X-ray scattering analysis. *J. Phys. Lett.*, **45**, 719.
21. Descamps, M., Correia, N.T., Derollez, P., Danede, F., and Capet, F. (2005) Plastic and glassy crystal states of caffeine. *J. Phys. Chem. B*, **109**, 16092.
22. Derollez, P., Correia, N.T., Danède, F., Capet, F., Affouard, F., Lefebvre, J., and Descamps, M. (2005) Ab initio structure determination of the high-temperature phase of anhydrous caffeine by X-ray powder diffraction. *Acta Crystallogr., Sect. B: Struct. Sci.*, **61**, 329.
23. Stevenson, C.L., Bennett, D.B., and Lechuga-Ballesteros, D. (2005) Pharmaceutical liquid crystals: the relevance of partially ordered systems. *J. Pharm. Sci.*, **94**, 1861.
24. Ziman, J. (1979) *Model of Disorder: The Theoretical Physics of Homogeneously Disordered Systems*, Cambridge University Press, New York.
25. Descamps, M. and Coulon, G. (1977) Series expansion calculation of the elastic neutron diffuse scattering: ice Ih. *Chem. Phys.*, **25**, 117.
26. Suchod, B. and Lajzerowicz-Bonneteau, J. (1991) Interactions between substitutional and orientational orders – the phase-transitions in enantiomeric and racemic crystals of tmhp. 1. X-ray structural studies of the orientational order-disorder transition in enantiomeric tmhp. *J. Phys. I*, **1**, 553.
27. Elarby, A., Jal, J.F., Dupuy, J., Chieux, P., Wright, A., and Parreins, R. (1982) Nucléation homogène et cristallisation delaglace cubique (Ic) dans les verres d'électrolytes LiCl.D2O, *Journal de Physique Lettres*, **43**, 355.
28. Proffen, T., Billinge, S.J.L., Egami, T., and Louca, D. (2003) Structural analysis of complex materials using the atomic pair distribution function – a practical guide. *Z. Kristallogr.*, **218**, 132.
29. Dmowski, W. and Swider-Lyons, K.E. (2004) PDF analysis – from atomic displacements to nanocrystals. *Z. Kristallogr.*, **219**, 136.
30. Kodama, K., Iikubo, S., Taguchi, T., and Shamoto, S.I. (2006) Finite size effects of nanoparticles on the atomic pair distribution functions. *Acta Crystallogr., Sect. A: Found. Crystallogr.*, **62**, 444.
31. Pauchet, M., Gervais, C., Courvoisier, L., and Coquerel, G. (2004) Successful application of the derived crystal packing (DCP) model in resolving the crystal structure of a metastable polymorph of (±) modafinil†. *Cryst. Growth Des.*, **4**, 1143.
32. Descamps, M., Legrand, V., Guinet, Y., Amazzal, A., Alba, C., and Dore, J. (1997) "Pre-peak" in the structure factor of simple molecular glass formers. *Prog. Theor. Phys. Suppl.*, **126**, 207.
33. Morineau, D. and Alba-Simionesco, C. (1998) Hydrogen-bond-induced clustering in the fragile glass-forming liquid m-toluidine: experiments and simulations. *J. Chem. Phys.*, **109**, 8494.
34. Qi, S., Weuts, I., De Cort, S., Stokbroekx, S., Leemans, R., Reading, M., Belton, P., and Craig, D.Q.M. (2010) An investigation into the crystallisation behaviour of an amorphous cryomilled pharmaceutical material above and below the glass transition temperature. *J. Pharm. Sci.*, **99**, 196.
35. Descamps, M. and Dudognon, E. (2014) Crystallization from the amorphous state: nucleation-growth decoupling, polymorphism interplay, and the role of interfaces. *J. Pharm. Sci.*, **103**, 2615.
36. Porter, D.A., Easterling, K.E., and Sherif, M. (2009) *Phase Transformations in Metals and Alloys*, 3rd (Revised Reprint) edn, Taylor & Francis.
37. Andronis, V. and Zografi, G. (2000) Crystal nucleation and growth of indomethacin polymorphs from the amorphous state. *J. Non-Cryst.-Solids*, **271**, 236.
38. Carpentier, L., Desprez, S., and Descamps, M. (2003) Crystallization and glass properties of pentitols: xylitol,

adonitol arabitol. *J. Therm. Anal.*, **73**, 577.
39. Legrand, V., Descamps, M., and Alba-Simionesco, C. (1997) Glass-forming meta-toluidine: a thermal and structural analysis of its crystalline polymorphism and devitrification. *Thermochim. Acta*, **307**, 77.
40. Kelton, K.F. (1991) Crystal nucleation in liquids and glasses. *Solid State Phys.*, **45**, 75.
41. Christian, J. (1975) *The Theory of Transformations in Metals and Alloys*, Pergamon Press, Oxford.
42. Debenedetti, P.G. (1996) *Metastable Liquids – Concepts and Principles*, Princeton University Press.
43. Gutzow, I. (1977) The mechanism of crystal growth in glass forming systems. *J. Cryst. Growth*, **42**, 15.
44. Gutzow, I. (1980) Kinetics of crystallization processes in glass forming melts. *J. Cryst. Growth*, **48**, 589.
45. Turnbull, D. (1956) *Solid State Physics – Advances in Research and Applications*, vol. **3**, Academic Press, p. 225.
46. Spaepen, F. (1975) A structural model for the solid-liquid interface in monatomic systems. *Acta Metall.*, **23**, 729.
47. Oxtoby, D.W. and Haymet, A.D.J. (1981) A molecular theory of the solid-liquid interface. II. Study of bcc crystal-melt interfaces. *J. Chem. Phys.*, **76**, 6262.
48. Spaepen, F. and Meyer, R.B. (1976) The surface tension in a structural model for the solid-liquid interface. *Scr. Metall.*, **10**, 257.
49. Descamps, M. and Decroix, A.A. (2014) Polymorphism and disorder in caffeine: dielectric investigation of molecular mobilities. *J. Mol. Struct.*, **1078**, 165.
50. Ostwald, W. (1897) Studien über die Bildung und Umwandlung fester Körper. *Z. Angew. Phys.*, **22**, 289.
51. Threlfall, T. (2003) Structural and thermodynamic explanations of ostwald's rule. *Org. Process Res. Dev.*, **7**, 1017.
52. Dudognon, E., Correia, N.T., Danède, F., and Descamps, M. (2013) Solid-solid transformation in racemic Ibuprofen. *Pharm. Res.*, **30**, 81.
53. Dudognon, E., Danède, F., Descamps, M., and Correia, N.T. (2008) Evidence for a new crystalline phase of racemic Ibuprofen. *Pharm. Res.*, **25**, 2853.
54. Zhu, L., Brian, C.W., Swallen, S.F., Straus, P.T., Ediger, M.D., and Yu, L. (2011) Surface self-diffusion of an organic glass. *Phys. Rev. Lett.*, **106**.
55. Capaccioli, S., Ngai, K.L., Paluch, M., and Prevosto, D. (2012) Mechanism of fast surface self-diffusion of an organic glass. *Phys. Rev. E: Stat. Nonlinear Soft Matter Phys.*, **86**.
56. Alonzo, D.E., Gao, Y., Zhou, D., Mo, H., Zhang, G.G., and Taylor, L.S. (2011) Dissolution and precipitation behavior of amorphous solid dispersions. *J. Pharm. Sci.*, **100**, 3316.
57. Alonzo, D.E., Zhang, G.G.Z., Zhou, D., Gao, Y., and Taylor, L.S. (2010) Understanding the behavior of amorphous pharmaceutical systems during dissolution. *Pharm. Res.*, **27**, 608.
58. Newman, A., Knipp, G., and Zografi, G. (2012) Assessing the performance of amorphous solid dispersions. *J. Pharm. Sci.*, **101**, 1355.
59. Qi, S., McAuley, W.J., Yang, Z., and Tipduangta, P. (2014) Physical stabilization of low-molecular-weight amorphous drugs in the solid state: a material science approach. *Ther. Delivery*, **5**, 817.
60. Dahan, A., Beig, A., Ioffe-Dahan, V., Agbaria, R., and Miller, J.M. (2013) The twofold advantage of the amorphous form as an oral drug delivery practice for lipophilic compounds: Increased apparent solubility and drug flux through the intestinal membrane. *AAPS J.*, **15**, 347.
61. Frank, K.J., Rosenblatt, K.M., Westedt, U., Hölig, P., Rosenberg, J., Mägerlein, M., Fricker, G., and Brandl, M. (2012) Amorphous solid dispersion enhances permeation of poorly soluble ABT-102: true supersaturation vs. apparent solubility enhancement. *Int. J. Pharm.*, **437**, 288.
62. Gardner, C.R., Walsh, C.T., and Almarsson, Ö. (2004) Drugs as materials: valuing physical form in drug discovery. *Nat. Rev. Drug Discovery*, **3**, 926.

63. Miller, J.M., Beig, A., Carr, R.A., Spence, J.K., and Dahan, A. (2012) A win-win solution in oral delivery of lipophilic drugs: supersaturation via amorphous solid dispersions increases apparent solubility without sacrifice of intestinal membrane permeability. *Mol. Pharm.*, **9**, 2009.
64. Kittel, C. and Kroemer, H. (1980) *Thermal Physics*, W. H. Freeman.
65. Amharar, Y., Curtin, V., Gallagher, K.H., and Healy, A.M. (2014) Solubility of crystalline organic compounds in high and low molecular weight amorphous matrices above and below the glass transition by zero enthalpy extrapolation. *Int. J. Pharm.*, **472**, 241.
66. Ilevbare, G.A. and Taylor, L.S. (2013) Liquid-liquid phase separation in highly supersaturated aqueous solutions of poorly water-soluble drugs: implications for solubility enhancing formulations. *Cryst. Growth Des.*, **13**, 1497.
67. Angell, C.A. (1988) Perspective on the glass transition. *J. Phys. Chem.*, **49**, 863.
68. Jäckle, J. (1986) Models of the glass transition. *Rep. Prog. Phys.*, **49** (2), 171.
69. Debenedetti, P.G. and Stillinger, F.H. (2001) Supercooled liquids and the glass transition. *Nature*, **410**, 259.
70. Willart, J.F. and Descamps, M. (2008) Solid state amorphization of pharmaceuticals. *Mol. Pharm.*, **5**, 905.
71. Angell, C.A. (1995) Formation of glasses from liquids and biopolymers. *Science*, **267**, 1924.
72. Goldstein, M. (1976) Viscous liquids and the glass transition. V. Sources of the excess specific heat of the liquid. *J. Chem. Phys.*, **64**, 4767.
73. Angell, C.A. (1995) The old problems of glass and the glass transition, and the many new twists. *Proc. Natl. Acad. Sci. U.S.A.*, **92**, 6675.
74. Hodge, I.M. (1996) Strong and fragile liquids – a brief critique. *J. Non-Cryst. Solids*, **202**, 164.
75. Angell, C.A., McMillan, P.F., Oganov, A.R., and Wolynes, P.G. (2005) Energy landscapes for cooperative processes: nearly ideal glass transitions, liquid-liquid transitions and folding transitions. *Philos. Trans. R. Soc. A: Math. Phys. Eng. Sci.*, **363**, 415.
76. Angell, C.A. (2008) Glass-formers and viscous liquid slowdown since David turnbull: enduring puzzles and new twists. *MRS Bull.*, **33**, 544.
77. Descamps, M., Moura Ramos, J.J., and Correia, N.T. (2002) Ageing exploration of the energy landscape of a glass by the TSDC technique. *Mol. Phys.*, **100**, 2669.
78. Kauzmann, W. (1948) The nature of the glassy state and the behavior of liquids at low temperatures. *Chem. Rev.*, **43**, 219.
79. Adam, G. and Gibbs, J.H. (1965) On the temperature dependence of cooperative relaxation properties in glass-forming liquids. *J. Chem. Phys.*, **43**, 139.
80. Stillinger, F.H. (1988) Supercooled liquids, glass transitions, and the Kauzmann paradox. *J. Chem. Phys.*, **88**, 7818.
81. Dyre, J.C. (2006) Colloquium: the glass transition and elastic models of glass-forming liquids. *Rev. Mod. Phys.*, **78**, 953.
82. Ediger, M.D., Angell, C.A., and Nagel, S.R. (1996) Supercooled liquids and glasses. *J. Phys. Chem.*, **100**, 13200.
83. Angell, C.A., Ngai, K.L., McKenna, G.B., McMillan, P.F., and Martin, S.W. (2000) Relaxation in glassforming liquids and amorphous solids. *J. Appl. Phys.*, **88**, 3113.
84. Mauro, J.C. (2014) Grand challenges in glass science. *Front. Mater.*, **1**, 20.
85. Carpentier, L., Decressain, R., Desprez, S., and Descamps, M. (2006) Dynamics of the amorphous and crystalline α-, β-phases of indomethacin. *J. Phys. Chem. B*, **110**, 457.
86. Wojnarowska, Z., Adrjanowicz, K., Wlodarczyk, P., Kaminska, E., Kaminski, K., Grzybowska, K., Wrzalik, R., Paluch, M., and Ngai, K.L. (2009) Broadband dielectric relaxation study at ambient and elevated pressure of molecular dynamics of pharmaceutical: indomethacin. *J. Phys. Chem. B*, **113**, 12536.

87. Busch, R. (2000) Thermophysical properties of bulk metallic glass-forming liquids. *JOM*, **52**, 39.
88. Angell, C.A. (1997) Why C1 = 16-17 in the WLF equation is physical – and the fragility of polymers. *Polymer*, **38**, 6261.
89. Donth, E. (1996) Characteristic length of the glass transition. *J. Polym. Sci., Part B: Polym. Phys.*, **34**, 2881.
90. Stevenson, J.D., Schmalian, J., and Wolynes, P.G. (2006) The shapes of cooperatively rearranging regions in glass forming liquids. *Nat. Phys.*, **21**, 268.
91. Williams, G. and Watts, D.C. (1970) Non-symmetrical dielectric relaxation behaviour arising from a simple empirical decay function. *Trans. Faraday Soc.*, **66**, 80.
92. Böhmer, R., Ngai, K.L., Angell, C.A., and Plazek, D.J. (1993) Nonexponential relaxations in strong and fragile glass formers. *J. Chem. Phys.*, **99**, 4201.
93. Böhmer, R. and Angell, C.A. (1994) in *Disorder Effects on Relaxational Processes* (eds R. Richert and A. Blumen), Springer, Berlin, Heidelberg, p. 11.
94. Richert, R. (2002) Heterogeneous dynamics in liquids: fluctuations in space and time. *J. Phys.: Condens. Matter*, **14**, R703.
95. Ngai, K.L. (2011) *Relaxation and Diffusion in Complex Systems*, Springer, New York.
96. Correia, N.T., Moura Ramos, J.J., Descamps, M., and Collins, G. (2001) Molecular mobility and fragility in indomethacin: a thermally stimulated depolarization current study. *Pharm. Res.*, **18**, 1767.
97. Lunkenheimer, P., Wehn, R., Schneider, U., and Loidl, A. (2005) Glassy aging dynamics. *Phys. Rev. Lett.*, **95**.
98. Tool, A.Q. and Eicitlin, C.G. (1931) Variations caused in the heating curves of glass by heat treatment. *J. Am. Ceram. Soc.*, **14**, 276.
99. de Bast, J. and Gilard, P. (1963) Variation of the viscosity of glass and relaxation of stresses during stabilization. *Phys. Chem. Glasses*, **4**, 117.
100. Struik, L.C.E. (1977) Physical aging in plastics and other glassy materials. *Polym. Eng. Sci.*, **17**, 165.
101. Moynihan, C.T., Easteal, A.J., DeBolt, M.A., and Tucker, J. (1976) Dependence of the fictive temperature of glass on cooling rate. *J. Am. Ceram. Soc.*, **59**, 12.
102. Pappin, A.J., Hutchinson, J.M., and Ingram, M.D. (1992) Enthalpy relaxation in polymer glasses: evaluation and interpretation of the tool-narayanaswamy parameter x for poly(vinyl chloride). *Macromolecules*, **25**, 1084.
103. Hodge, I.M. (1994) Enthalpy relaxation and recovery in amorphous materials. *J. Non-Cryst. Solids*, **169**, 211.
104. Hodge, I.M. (1997) Adam-Gibbs formulation of enthalpy relaxation near the glass transition. *J. Res. Nat. Inst. Stand. Technol.*, **102**, 195.
105. Hodge, I.M. (2013) Parameterization of annealing kinetics in pharmaceutical glasses. *J. Pharm. Sci.*, **102**, 2235.
106. Luthra, S.A., Hodge, I.M., and Pikal, M.J. (2008) Effects of annealing on enthalpy relaxation in lyophilized disaccharide formulations: mathematical modeling of DSC curves. *J. Pharm. Sci.*, **97**, 3084.
107. Johari, G.P. and Goldstein, M. (1970) Viscous liquids and the glass transition. II. Secondary relaxations in glasses of rigid molecules. *J. Chem. Phys.*, **53**, 2372.
108. Carpentier, L. and Descamps, M. (2003) Dynamic decoupling and molecular complexity of flass-forming maltitol. *J. Phys. Chem. B*, **107**, 271.
109. Ngai, K.L. and Paluch, M. (2004) Classification of secondary relaxation in glass-formers based on dynamic properties. *J. Chem. Phys.*, **120**, 857.
110. Johari, G.P. (1973) Intrinsic mobility of molecular glasses. *J. Chem. Phys.*, **58**, 1766.
111. Reid, C.J. and Evans, M.W. (1979) Zero-THz absorption profiles in glassy solutions. High frequency γ process and its characterisation. *J. Chem. Soc., Faraday Trans. 2*, **75**, 1218.
112. Goldstein, M. (1969) Viscous liquids and the glass transition: a potential

energy barrier picture. *J. Chem. Phys.*, **51**, 3728.

113. Stillinger, F.H. (1995) A topographic view of supercooled liquids and glass formation. *Science*, **267**, 1935.
114. Stanley, H.E., Kumar, P., Franzese, G., Xu, L., Yan, Z., Mazza, M.G., Buldyrev, S.V., Chen, S.H., and Mallamace, F. (2008) Liquid polyamorphism: possible relation to the anomalous behaviour of water. *Eur. Phys. J.: Spec. Top.*, **161**, 1.
115. Mishima, O. and Stanley, H.E. (1998) The relationship between liquid, supercooled and glassy water. *Nature*, **396**, 329.
116. Shalaev, E. and Zografi, G. (2002) in *Progress in Amorphous Food and Pharmaceutical Systems*, vol. **23** (ed H. Levine), The Royal Chemistry Society, p. 11.
117. Cohen, I., Ha, A., Zhao, X., Lee, M., Fischer, T., Strouse, M.J., and Kivelson, D. (1996) A low-temperature amorphous phase in a fragile glass-forming substance. *J. Phys. Chem.*, **100**, 8518.
118. Hédoux, A., Guinet, Y., Derollez, P., Hernandez, O., Lefort, R., and Descamps, M. (2004) A contribution to the understanding of the polyamorphism situation in triphenyl phosphite. *Phys. Chem. Chem. Phys.*, **6**, 3192.
119. Hédoux, A., Guinet, Y., Derollez, P., Hernandez, O., Paccou, L., and Descamps, M. (2006) Micro-structural investigations in the glacial state of triphenyl phosphite. *J. Non-Cryst. Solids*, **352**, 4994.